Hyperbolic reformulation of a 1D viscoelastic blood flow model and ADER finite volume schemes

Gino I. Montecinos, Lucas O. Müller and Eleuterio F. Toro

Laboratory of Applied Mathematics
DICAM
University of Trento
Trento, Italy
e-mail: gino.montecinos@unitn.it, lucas.mueller@unitn.it, toro@ing.unitn.it

February 4, 2014

Abstract

The applicability of ADER finite volume methods to solve hyperbolic balance laws with stiff source terms in the context of well-balanced and non-conservative schemes is extended to solve a one-dimensional blood flow model for viscoelastic vessels, reformulated as a hyperbolic system, via a relaxation time. A criterion for selecting relaxation times is found and an empirical convergence rate assessment is carried out to support this result. The proposed methodology is validated by applying it to a network of viscoelastic vessels for which experimental and numerical results are available. The agreement between the results obtained in the present paper and those available in the literature is satisfactory. Key features of the present formulation and numerical methodologies, such as accuracy, efficiency and robustness, are fully discussed in the paper.

Introduction

The validity of one-dimensional blood flow models for reproducing pressure and flow rate waveforms in the cardiovascular system has been confirmed in multiple ways. It has been shown that these models well reproduce pressure and flow rate waves obtained using three-dimensional computational models in real vascular geometries using both, rigid boundaries, see Grinberg *et al.* [29] and fully three-dimensional Fluid-Structure-Interaction (FSI) models, see Xiao *et al.* [64]. One-dimensional blood flow models have also shown to reproduce measured pressure and flow rate wave patterns in animal arteries Steele *et al.* [54], human arteries Reymond *et al* [51] and human veins Müeller and Toro [43]. Moreover, these models have been used to study a variety of pathological conditions, like the assessment of variations and occlusions of the Circle of Willis, see Alastruey *et al.* [3] or the study of the influence of aortic valve stenosis in systemic circulation, see Liang *et al.* [38]. Another relevant application of one-dimensional models is to provide boundary conditions for three-dimensional FSI models, see Blanco *et al.* [6].

In this paper we solve a time-dependent, one-dimensional system that is a model for blood flow in vessels with walls having viscoelastic properties. First, we reformulate the original Advection-Diffusion-Reaction (ADR) problem via a relaxation technique introduced by Cattaneo [13, 14],

obtaining a hyperbolic system with stiff source terms. Then, we solve the resulting system using appropriate high-order accurate numerical methods.

Cattaneo [13] and Vernotte [63] are credited for having introduced a relaxation technique for the heat equation, as a strategy for resolving the paradox of instantaneous wave propagation. See also Nagy et al. [44]. The relaxation approach consists of augmenting the Fourier law with a transient term involving a relaxation time, a parameter, which recovers the original Fourier law for small relaxation times. Even though this relaxation technique was originally developed to avoid a non-physical description of instantaneous heat propagation, it is also appropriate for the construction of numerical schemes that transform ADR equations into hyperbolic systems which may be stiff for small relaxation parameters.

Relaxation in the sense of Cattaneo has been applied to solve ADR problems, see for example Gómez and collaborators [28, 27], where two-dimensional implementations have been carried out for linear problems in the frame of finite element methods. Nishikawa and Roe [47, 48] and subsequently Nishikawa [45, 46] have implemented this approach in the frame of residual distribution schemes to find steady state solutions to parabolic partial differential equations.

We remark that there exist other relaxation approaches, as for example the one due to Jin *et al.* [34], which is an extension of the relaxation strategy presented by Jin and Xin [35], initially proposed to cast non-linear hyperbolic problems into linear hyperbolic systems with stiff source terms. However, this form of relaxation imposes a sub-characteristic condition for the derived hyperbolic systems and spurious oscillations appear when this condition is not ensured [1]. This relaxation approach also requires the sub-characteristic condition when applied to ADR problems, requiring small relaxation parameters. Furthermore, the relaxation parameter for the ADR case is present in the advective components. Therefore, stability depends on the relaxation. In the context of implicit-explicit methods [50, 7, 8], the influence of these parameters on the stability has been reduced by introducing an artificial viscosity. However, the accuracy of these methods is reached in the parabolic limit of the ADR equations, *i.e.* for very small relaxation parameters.

Here we make use of Cattaneo's relaxation technique because; i) avoids the sub-characteristic condition [35, 34] and therefore allows a large enough relaxation parameter suitable for numerical implementations; ii) allows selective relaxation of specific terms, in order to remove second order derivatives present in the original model requiring only minor changes in the mathematical formulation of the problem, maintaining the physical meaning of the relaxed model and allowing for larger relaxation parameters in comparison to alternative approaches; iii) allows to compute accurate and efficient solutions by implementing numerical schemes able to handle stiff source terms.

The hyperbolic system obtained by relaxation of the original ADR system contains a stiff source term. The numerical methods implemented here make use of the methodology presented by Müller and Toro [42], which proposes high-order ADER (**A**rbitrary Accuracy **DER**ivative Riemann problem) schemes for one-dimensional blood flow models, which reconcile source term stiffness, well-balanced properties, accuracy and stability. The ADER approach was put forward by Toro *et al.* [60] for linear problems on Cartesian meshes. Nowadays ADER schemes can be implemented in both the finite volume and discontinuous Galerkin finite element frameworks. ADER schemes are arbitrarily accurate in both space and time and are applicable to general geometries in multiple space dimensions. ADER schemes have recently been implemented to solve one-dimensional blood flow models for elastic vessels with varying geometrical and mechanical properties [42, 41] in the context of non-conservative hyperbolic systems. Moreover, ADER schemes have been applied to ADR equations. Titarev and Toro [56] extended the ADER methodology in a straightforward fashion to solve the model advection-diffusion equation. See also Toro and Hidalgo [59] and Hidalgo *et al.* [32] for applications of ADER to pure diffusion equations. ADER was applied to the compressible Navier-Stokes equations by Dumbser [18] and by Hidalgo and Dumbser in [31]. A

disadvantage of the approach used in the above cited works is the time stability constraint that scales with Δx^2, instead of the classical scaling of ADER schemes for hyperbolic problems, which is Δx. In this paper we relax this restriction exploiting the fact that ADER schemes can efficiently treat stiff source terms and are thus an excellent candidate to solve ADR equations using the hyperbolisation approach. For an introduction to ADER schemes and a review of the literature see chapters 19 and 20 of [58].

This paper is organised as follows. The governing equations, the relaxation procedure and the blood flow model and its hyperbolic reformulation are presented in section 1. In section 2 we briefly introduce the concepts of the ADER approach and the numerical methodology used in this work. In section 3, we propose a sufficiency criterion for defining the relaxation time in such a way that ensures that the formulation error will be smaller than the spatial discretization error and provide numerical evidence that confirms the proposed criterion. In section 4 we validate the proposed methodology by comparing our numerical results with experimental measurements and numerical results reported in the literature for one-dimensional blood flow in a network of viscoelastic vessels. Conclusions and remarks are drawn in section 5.

1 Governing equations

We consider non-linear advection-diffusion-reaction (ADR) equations written in the form

$$\partial_t \mathbf{Q} + \mathbf{A}(\mathbf{Q})\partial_x \mathbf{Q} = \partial_x \mathbf{G}(\mathbf{Q}, \partial_x \mathbf{Q}) + \mathbf{S}(\mathbf{Q}) \,. \tag{1}$$

Here, $\mathbf{Q} \in \mathbb{R}^m$ is the vector of unknowns; $\mathbf{A}(\mathbf{Q})$ is a matrix; $\mathbf{G}(\mathbf{Q}, \partial_x \mathbf{Q})$ represents the viscous flux and $\mathbf{S}(\mathbf{Q})$ is the reaction term, a function of the unknown.

We introduce the following matrices

$$\mathbf{B}(\mathbf{Q}, \partial_x \mathbf{Q}) = \frac{\partial \mathbf{G}(\mathbf{Q}, \partial_x \mathbf{Q})}{\partial \mathbf{Q}} \,, \quad \mathbf{D}(\mathbf{Q}, \partial_x \mathbf{Q}) = \frac{\partial \mathbf{G}(\mathbf{Q}, \partial_x \mathbf{Q})}{\partial (\partial_x \mathbf{Q})} \,. \tag{2}$$

With these definitions we can write the governing equations as

$$\partial_t \mathbf{Q} + \Big(\mathbf{A}(\mathbf{Q}) - \mathbf{B}(\mathbf{Q}, \partial_x \mathbf{Q})\Big)\partial_x \mathbf{Q} = \mathbf{D}(\mathbf{Q}, \partial_x \mathbf{Q})\partial_x^{(2)} \mathbf{Q} + \mathbf{S}(\mathbf{Q}) \,. \tag{3}$$

1.1 General formulation

We will relax system (3) by following the constitutive Cattaneo's law [13],

$$\partial_t \mathbf{U} - \tfrac{1}{\varepsilon}\partial_x \mathbf{Q} \;=\; -\tfrac{1}{\varepsilon}\mathbf{U} \,, \tag{4}$$

where $\varepsilon > 0$ is a parameter. In practice, the strategy introduces the new variable $\mathbf{U}$ instead of gradients $\partial_x \mathbf{Q}$ for selected terms of the original ADR equations. The evolution equation (4) for these new variables gives an asymptotic behaviour toward the original gradient. This allows to write (3) as

$$\partial_t \mathbf{Q} + \Big(\mathbf{A}(\mathbf{Q}) - \mathbf{B}(\mathbf{Q}, \mathbf{U})\Big)\partial_x \mathbf{Q} = \mathbf{D}(\mathbf{Q}, \mathbf{U})\partial_x \mathbf{U} + \mathbf{S}(\mathbf{Q}) \,. \tag{5}$$

We only consider components of $\mathbf{U}$ as the non-zero components i of $\partial_x \mathbf{Q}$ such that the i-th column of $\mathbf{D}$ in (2) is not null. If we consider $n \leq m$ columns of $\mathbf{D}$ to be not null then, we can consider $\mathbf{U} \in \mathbb{R}^n$ and

$$\begin{aligned} \partial_t \mathbf{Q} + \Big(\mathbf{A}(\mathbf{Q}) - \mathbf{B}(\mathbf{Q}, \mathbf{U})\Big)\partial_x \mathbf{Q} &= \mathbf{D}(\mathbf{Q}, \mathbf{U})\partial_x \mathbf{U} + \mathbf{S}(\mathbf{Q}) \,. \\ \partial_t \mathbf{U} - \tfrac{1}{\varepsilon}\partial_x \mathbf{Q} &= -\tfrac{1}{\varepsilon}\mathbf{U} \,. \end{aligned} \tag{6}$$

System (6) written in a semilinear form gives

$$\partial_t \mathbf{W} + \mathbf{J}(\mathbf{Q})\partial_x \mathbf{W} = \mathbf{L}(\mathbf{W}), \tag{7}$$

where

$$\mathbf{W} = \begin{bmatrix} \mathbf{Q} \\ \mathbf{U} \end{bmatrix}, \quad \mathbf{J}(\mathbf{W}) = \begin{bmatrix} \mathbf{A}-\mathbf{B} & -\bar{\mathbf{D}} \\ -\frac{1}{\varepsilon}\mathbf{I} & \mathbf{0} \end{bmatrix}, \quad \mathbf{L}(\mathbf{W}) = \begin{bmatrix} \mathbf{S}(\mathbf{Q}) \\ -\frac{1}{\varepsilon}\mathbf{U} \end{bmatrix}, \tag{8}$$

with matrix $\bar{\mathbf{D}} \in \mathbb{R}^{m\times n}$ containing only the n not null column vectors of $\mathbf{D}$, $\mathbf{I}$ is the identity matrix in $\mathbb{R}^{n\times n}$ and $\mathbf{0}$ is the null matrix in $\mathbb{R}^{n\times m}$.

1.2 One-dimensional blood flow model for viscoelastic vessels

Let us consider well-known equations that describe one-dimensional blood flow as in [42]

$$\left.\begin{aligned} \partial_t A(x,t) + \partial_x q(x,t) &= 0, \\ \partial_t q(x,t) + \partial_x\left(\hat{\alpha}\frac{q(x,t)^2}{A(x,t)}\right) + \frac{A(x,t)}{\rho}\partial_x p(x,t) &= f(x,t), \end{aligned}\right\} \tag{9}$$

where x is the axial coordinate along the vessel, t is time, $A(x,t)$ is the cross-sectional area, $q(x,t)$ is the flow rate, $\hat{\alpha} \equiv 1$, which indicates a blunt velocity profile, ρ is the fluid density, assumed as a constant, $p(x,t)$ is the average internal pressure and $f(x,t)$ is the friction force per unit length, given by

$$f(x,t) = -\gamma\pi\nu\frac{q}{A}, \tag{10}$$

where ν is the kinematic viscosity. In this work we take $\gamma = 22$, as specified in [2].

To close system (9) we introduce an additional equation known as tube law

$$p = p_e + \psi(A, A_0, K) + \varphi(A, A_0)\partial_t A, \tag{11}$$

where $p_e(x,t)$ is the external pressure and ψ is the transmural pressure given by

$$\psi(A(x,t), A_0(x), K(x)) = K(x)\phi(A(x,t), A_0(x)),$$

with

$$\phi(A(x,t), A_0(x)) = \left(\left(\frac{A(x,t)}{A_0(x)}\right)^m - \left(\frac{A(x,t)}{A_0(x)}\right)^n\right). \tag{12}$$

$A_0(x)$ is the cross-sectional area at equilibrium, $K(x)$ is a positive function which depends on the Young modulus, the wall thickness and A_0, with $m > 0$ and $n \in (-2, 0]$. See [9] for details.

Moreover, the viscoelastic term $\varphi(A, A_0)\partial_t A$, taken as in [2], is

$$\varphi(A, A_0) = \frac{\Gamma}{A_0\sqrt{A}}, \tag{13}$$

where Γ is a constant related to the viscoelastic properties of the vessel wall.

From the governing equations we obtain $\partial_t A = -\partial_x q$, allowing us to write

$$p = p_e + \psi(A, A_0, K) - \varphi(A, A_0)\partial_x q. \tag{14}$$

The pressure gradient is thus

$$\begin{aligned} \partial_x p \quad = \quad & [1]\partial_x p_e + [\phi]\partial_x K + \left[K(\partial_A\phi) - (\partial_A\varphi)(\partial_x q)\right]\partial_x A \\ & + \left[K(\partial_{A_0}\phi) - (\partial_{A_0}\varphi)(\partial_x q)\right]\partial_x A_0 - [\varphi]\partial_x^{(2)} q. \end{aligned} \tag{15}$$

1.3 Hyperbolic reformulation of the equations

Following Toro and Siviglia [61], we write system (9) with viscoelastic tube law (11) as

$$\left.\begin{array}{rcl} \partial_t A(x,t) + \partial_x q(x,t) & = & 0\,, \\ \partial_t q(x,t) + \partial_x \left(\hat{\alpha} \dfrac{q(x,t)^2}{A(x,t)} \right) & = & -\left[\frac{A}{\rho}\right] \partial_x p_e - \left[\frac{A}{\rho}\phi\right] \partial_x K \\ & & -\frac{A}{\rho}\left[K(\partial_A \phi) - (\partial_A \varphi)(\partial_x q)\right] \partial_x A \\ & & -\frac{A}{\rho}\left[K(\partial_{A_0} \phi) - (\partial_{A_0} \varphi)(\partial_x q)\right] \partial_x A_0 \\ & & +\frac{A}{\rho}\left[\varphi\right] \partial_x^{(2)} q + f\,, \\ \partial_t K & = & 0\,, \\ \partial_t A_0 & = & 0\,, \\ \partial_t p_e & = & 0\,, \end{array}\right\} \tag{16}$$

which can be written as (1) with the following definitions

$$\left.\begin{array}{c} \mathbf{Q} = \left[\begin{array}{ccccc} A & q & K & A_0 & p_e \end{array}\right]^T, \\ \\ \mathbf{A} = \left[\begin{array}{ccccc} 0 & 1 & 0 & 0 & 0 \\ c^2 - u^2 + \frac{\varphi \partial_x q}{2\rho} & 2u & \frac{A}{\rho}\phi & \frac{A}{A_0}\left(\frac{\varphi \partial_x q}{\rho} - c^2\right) & \frac{A}{\rho} \\ 0 & 0 & 0 & 0 & 0 \\ 0 & 0 & 0 & 0 & 0 \\ 0 & 0 & 0 & 0 & 0 \end{array}\right], \\ \\ \mathbf{S} = \left[\begin{array}{ccccc} 0 & f & 0 & 0 & 0 \end{array}\right]^T, \\ \\ \partial_x \mathbf{G}(\mathbf{Q}, \partial_x \mathbf{Q}) = \left[\begin{array}{ccccc} 0 & \frac{\varphi A}{\rho} \partial_x^{(2)} q & 0 & 0 & 0 \end{array}\right]^T. \end{array}\right\} \tag{17}$$

We introduce a new variable Ψ and a relaxation parameter $\varepsilon > 0$ such that

$$\Psi \to \partial_x q\,,\ \varepsilon \to 0\,. \tag{18}$$

In addition, we mimic the Cattaneo's law [13] with an evolution equation for Ψ given by

$$\partial_t \Psi = \frac{1}{\varepsilon}(\partial_x q - \Psi)\,. \tag{19}$$

Therefore, we can reformulate system (16) as

$$\left.\begin{aligned}
\partial_t A(x,t)+\partial_x q(x,t) &= 0\,,\\
\partial_t q(x,t)+\partial_x\left(\hat{\alpha}\frac{q(x,t)^2}{A(x,t)}\right) &= -\left[\tfrac{A}{\rho}\right]\partial_x p_e-\left[\tfrac{A}{\rho}\phi\right]\partial_x K\\
&\quad -\tfrac{A}{\rho}\left[K(\partial_A\phi)-(\partial_A\varphi)\Psi\right]\partial_x A\\
&\quad -\tfrac{A}{\rho}\left[K(\partial_{A_0}\phi)-(\partial_{A_0}\varphi)\Psi\right]\partial_x A_0\\
&\quad -\tfrac{A}{\rho}\left[\varphi\right]\partial_x\Psi+f\,,\\
\partial_t K &= 0\,,\\
\partial_t A_0 &= 0\,,\\
\partial_t p_e &= 0\\
\partial_t\Psi+\tfrac{-1}{\varepsilon}\partial_x q &= -\tfrac{1}{\varepsilon}\Psi\,,
\end{aligned}\right\} \tag{20}$$

which can be written in quasi-linear form (7) with

$$\left.\begin{aligned}
\mathbf{W} &= \begin{bmatrix} A & q & K & A_0 & p_e & \Psi \end{bmatrix}^T,\\
\mathbf{J} &= \begin{bmatrix}
0 & 1 & 0 & 0 & 0 & 0\\
c^2-u^2+\frac{a_\Gamma}{2} & 2u & \frac{A}{\rho}\phi & \frac{A}{A_0}\left(a_\Gamma-c^2\right) & \frac{A}{\rho} & -\frac{A}{\rho}\varphi\\
0 & 0 & 0 & 0 & 0 & 0\\
0 & 0 & 0 & 0 & 0 & 0\\
0 & 0 & 0 & 0 & 0 & 0\\
0 & -\frac{1}{\varepsilon} & 0 & 0 & 0 & 0
\end{bmatrix},\\
\mathbf{L} &= \begin{bmatrix} 0 & f & 0 & 0 & 0 & -\frac{1}{\varepsilon}\Psi \end{bmatrix}^T,
\end{aligned}\right\} \tag{21}$$

where

$$c^2=\tfrac{A}{\rho}K\partial_A\phi\,,\quad u=\tfrac{q}{A}\,,\quad a_\Gamma=\tfrac{\varphi\Psi}{\rho}\,. \tag{22}$$

1.4 Eigenstructure

In this section we study the eigenstructure for the first order system (7) with Jacobian (21).

Proposition 1.1. *System (7) with Jacobian (21) is hyperbolic provided that*

$$\varepsilon^{-1}\geq-\frac{\Psi}{2A}-\frac{\rho\,c^2}{\varphi A}\,, \tag{23}$$

with eigenvalues

$$\lambda_1=u-\tilde{c}\,,\quad \lambda_2=\lambda_3=\lambda_4=\lambda_5=0\,,\quad \lambda_6=u+\tilde{c}, \tag{24}$$

where

$$\tilde{c}=\sqrt{c^2+\omega}\,,\quad \omega=\tfrac{\varphi A}{\rho\varepsilon}+\tfrac{a_\Gamma}{2} \tag{25}$$

and linear independent eigenvectors

$$\left.\begin{aligned}
\mathbf{v}_1 &= \begin{bmatrix} 1 \\ u-\tilde{c} \\ 0 \\ 0 \\ 0 \\ -\frac{1}{\varepsilon} \end{bmatrix}, \quad \mathbf{v}_6 = \begin{bmatrix} 1 \\ u+\tilde{c} \\ 0 \\ 0 \\ 0 \\ -\frac{1}{\varepsilon} \end{bmatrix}, \quad \mathbf{v}_2 = \begin{bmatrix} 1 \\ 0 \\ 0 \\ 0 \\ 0 \\ \frac{(c^2+a_\Gamma/2)-u^2}{\varphi A}\rho \end{bmatrix}, \\
\mathbf{v}_3 &= \begin{bmatrix} 0 \\ 0 \\ 1 \\ 0 \\ 0 \\ \frac{\phi}{\varphi} \end{bmatrix}, \quad \mathbf{v}_4 = \begin{bmatrix} 0 \\ 0 \\ 0 \\ 1 \\ 0 \\ \frac{(a_\Gamma-c^2)}{\varphi A_0}\rho \end{bmatrix}, \quad \mathbf{v}_5 = \begin{bmatrix} 0 \\ 0 \\ 0 \\ 0 \\ 1 \\ \frac{1}{\varphi} \end{bmatrix}.
\end{aligned}\right\} \tag{26}$$

Proof. (omitted) . □

Proposition 1.2. *Fields associated to eigenvectors* $\mathbf{v}_1$ *and* $\mathbf{v}_6$ *are genuinely non-linear.*

Proof. We denote $\lambda_1 = \lambda_-$ and $\lambda_6 = \lambda_+$. In a similar manner we redefine sub-indices of associated eigenvectors. The result follows by noting that

$$\nabla_{\mathbf{W}}\lambda_\pm \cdot \mathbf{v}_\pm = -\tfrac{1}{q} \pm \tfrac{1}{\tilde{c}}\left(c\tfrac{\partial c}{\partial A} + \tfrac{\partial \omega}{\partial A}\right) - (u \pm \tilde{c})\tfrac{A}{q^2} \pm \tfrac{1}{2\tilde{c}}\tfrac{\partial \omega}{\partial \Psi} \neq 0\,. \tag{27}$$

□

Proposition 1.3. *Fields associated to eigenvectors* $\mathbf{v}_2$ *to* $\mathbf{v}_5$ *are linearly-degenerated fields.*

Proof. The proof follows from the fact that for these eigenvectors, the associated eigenvalues are identically zero, so that

$$\nabla_{\mathbf{W}}\lambda = \mathbf{0}\,. \tag{28}$$

□

Proposition 1.4. *Let* $\mathcal{N}^1(\mathbf{W})$ *and* $\mathcal{N}^6(\mathbf{W})$ *be two functions of* $\mathbf{W}$*. Riemann invariants associated to genuinely non-linear fields for eigenvectors* $\mathbf{v}_1$ *and* $\mathbf{v}_6$ *satisfy*

$$\mathcal{N}^1 := u - \int \frac{\tilde{c}}{A}dA = constant\,, \quad \mathcal{N}^6 := u + \int \frac{\tilde{c}}{A}dA = constant, \tag{29}$$

respectively.

Proof. From eigenvectors associated to genuinely non-linear fields, the significant Riemann invariant for non-linear fields is

$$\frac{1}{dA} = \frac{u \pm \tilde{c}}{dq}\,. \tag{30}$$

By considering $uA = q$ and manipulating the above expression we obtain

$$du = \pm\frac{\tilde{c}}{A}dA \tag{31}$$

and the result holds. □

Proposition 1.5. *Let* $\mathfrak{L}^1(\mathbf{W})$ *and* $\mathfrak{L}^2(\mathbf{W})$ *functions of* $\mathbf{W}$*. For* p_e*,* A_0 *and* K *constants, Riemann invariants associated to linearly degenerate fields for eigenvectors* $\mathbf{v}_2$ *to* $\mathbf{v}_5$ *satisfy*

$$\mathfrak{L}^1 := \tilde{p} + \tfrac{1}{2}\rho u^2 = constant\,, \quad \mathfrak{L}^2 := q = constant\,, \tag{32}$$

with $\tilde{p} = p_e + \psi - \varphi\Psi$.

Proof. We note that for constant values of p_e, A_0 and K we can consider a reduced system of the form (7) with

$$\left.\begin{array}{c} \mathbf{W} = \left[\begin{array}{ccc} A & q & \Psi \end{array}\right]^T, \\ \mathbf{J} = \left[\begin{array}{ccc} 0 & 1 & 0 \\ c^2 - u^2 + \dfrac{a_\Gamma}{2} & 2u & -\frac{A}{\rho}\varphi \\ 0 & -\frac{1}{\varepsilon} & 0 \end{array}\right], \\ \mathbf{S} = \left[\begin{array}{ccc} 0 & f & -\frac{1}{\varepsilon}\Psi \end{array}\right]^T. \end{array}\right\} \tag{33}$$

This system has eigenvalues

$$\lambda_1 = u - \tilde{c}\,, \quad \lambda_2 = 0\,, \quad \lambda_3 = u + \tilde{c}\,. \tag{34}$$

Corresponding eigenvectors are

$$\mathbf{v}_1 = \left[\begin{array}{c} 1 \\ u - \tilde{c} \\ -\frac{1}{\varepsilon} \end{array}\right], \quad \mathbf{v}_2 = \left[\begin{array}{c} 1 \\ 0 \\ -\frac{\rho}{\varphi A}\left\{u^2 - (c^2 + a_\Gamma/2)\right\} \end{array}\right], \quad \mathbf{v}_3 = \left[\begin{array}{c} 1 \\ u + \tilde{c} \\ -\frac{1}{\varepsilon} \end{array}\right]. \tag{35}$$

Riemann invariants associated to the stationary contact discontinuity (characteristic field associated to the eigenvalue λ_2) are

$$\frac{1}{dA} = \frac{0}{dq} = \frac{-\frac{\rho}{\varphi A}\left\{u^2 - (c^2 + a_\Gamma/2)\right\}}{d\Psi}\,. \tag{36}$$

Hence, we obtain $\mathfrak{L}^2 = q = constant$ and

$$M(A,\Psi)d\Psi + N(A,\Psi)dA = 0\,, \tag{37}$$

with

$$M(A,\Psi) = \tfrac{A\varphi}{\rho}\,, \quad N(A,\Psi) = u^2 - c^2 + \tfrac{a_\Gamma}{\rho}\,. \tag{38}$$

This ordinary differential problem is not exact because

$$\frac{\partial M}{\partial A} \neq \frac{\partial N}{\partial \Psi}\,.$$

However, it can be proved that an integrating factor for this problem is $F(A) = \frac{1}{A}$, *i.e.*

$$\frac{\partial (FM)}{\partial A} = \frac{\partial (FN)}{\partial \Psi}\,.$$

Moreover, (37) is equivalent to

$$F(A)M(A,\Psi)d\Psi + F(A)N(A,\Psi)dA = 0\,. \tag{39}$$

Hence, the Riemann invariant is a function $\mathfrak{L}^1(A,\Psi)$ which satisfies $d\mathfrak{L}^1 = 0$ or

$$\begin{aligned} \partial_A \mathfrak{L}^1(A,\Psi) &= F(A)N(A,\Psi) = \tfrac{1}{A}\left(u^2 - c^2 - \tfrac{a_\Gamma}{2}\right), \\ \partial_\Psi \mathfrak{L}^1(A,\Psi) &= F(A)M(A) = \tfrac{\varphi}{\rho}\,. \end{aligned} \tag{40}$$

To find $\mathfrak{L}^1$ we first integrate $\partial_\Psi \mathfrak{L}^1$ in (40) with respect to Ψ which yields

$$\mathfrak{L}^1(A,\Psi) = a_\Gamma + g(A)\,. \tag{41}$$

Then, $g(A)$ is found by differentiating (41) with respect to A and using (40) to obtain

$$g'(A) = \frac{u^2 - c^2}{A}\,, \tag{42}$$

providing

$$\mathfrak{L}^1(A,\Psi) = a_\Gamma - \frac{\psi}{\rho} - \frac{u^2}{2}\,. \tag{43}$$

Since ρ is constant, from (37) and (39) we conclude that $\mathfrak{L}^1(A,\Psi)$ is constant across waves associated to linearly-degenerate fields. □

2 Numerical methods

The ADER methodology [60, 62, 55] consists of two main building blocks: a spatial reconstruction procedure and the solution of a generalised Riemann problem at each interface. ADER is, effectively, an extension of the second-order method of Ben-Artzi and Falcoviz [5]. The extension relates to the generalised Riemann problem and is twofold: (i) initial conditions are piece-wise smooth, for example piece-wise polynomials of any degree and (ii) source terms in the equations are included, if present originally. We also remark that ADER is akin to the method proposed by Harten et al. [30], as noted by Castro and Toro [12]. The ADER approach was first put forward by Toro et al. [60] for linear problems on Cartesian meshes, see also [52]. Several extensions have been proposed for non-linear problems on Cartesian [57] and non Cartesian meshes [36, 37, 11], to mention but a few. Extension of the ADER approach in the framework of discontinuous Galerkin finite element methods is due to Dumbser and collaborators; see [23, 16, 17], for instance. Subsequently, the ADER approach was extended to non-conservative balance laws [10, 20, 22, 24] to mention but a few. ADER methods are one-step schemes, fully discrete, containing two main ingredients: (i) a high-order spatial reconstruction procedure and (ii) the solution of a generalised, or high order, Riemann problem (GRP) at each cell interface. Reconstructions should be non-linear in order to circumvent Godunov's theorem [26, 58]. Concerning the GRP, in this paper we use the solver due to Dumbser et al. [21], that allows the treatment of stiff source terms in such a way that the usually contradictory requirements of high accuracy and stiffness are reconciled. For a review of ADER see [12, 40] and chapters 19 and 20 of [58].

2.1 ADER framework

We discretize the computational domain by a set of intervals $I_i = [x_{i-\frac{1}{2}}, x_{i+\frac{1}{2}}]$ of length $\Delta x = x_{i+\frac{1}{2}} - x_{i-\frac{1}{2}}$. Then we integrate (7) on the space-time cell, or volume, $I_i^n := I_i \times [t^n, t^{n+1}]$ which as shown in [20, 22] yields

$$\left.\begin{aligned} \mathbf{W}_i^{n+1} = & \quad \mathbf{W}_i^n + \frac{1}{\Delta x}\int_{t^n}^{t^{n+1}}\int_{x_{i-\frac{1}{2}}}^{x_{i+\frac{1}{2}}} \mathbf{J}(\mathbf{W}_i)\partial_x \mathbf{W}_i dx dt \\ & + \quad \frac{1}{\Delta x}\int_{t^n}^{t^{n+1}}\int_{x_{i-\frac{1}{2}}}^{x_{i+\frac{1}{2}}} \mathbf{L}(\mathbf{W}_i) dx dt \\ & - \quad \frac{\Delta t}{\Delta x}\left[\mathbf{D}^-_{i+\frac{1}{2}} + \mathbf{D}^+_{i-\frac{1}{2}}\right], \end{aligned}\right\} \tag{44}$$

with

$$\left.\begin{aligned} \mathbf{D}^-_{i+\frac{1}{2}} &= \frac{1}{\Delta t}\int_{t^n}^{t^{n+1}} \mathcal{D}^-_{i+\frac{1}{2}}(\mathbf{W}^-_{i+\frac{1}{2}}, \mathbf{W}^+_{i+\frac{1}{2}}) dt\,, \\ \mathbf{D}^+_{i-\frac{1}{2}} &= \frac{1}{\Delta t}\int_{t^n}^{t^{n+1}} \mathcal{D}^+_{i-\frac{1}{2}}(\mathbf{W}^-_{i-\frac{1}{2}}, \mathbf{W}^+_{i-\frac{1}{2}}) dt \end{aligned}\right\}. \tag{45}$$

Fluctuations $\mathcal{D}^{\pm}_{i+\frac{1}{2}}$ are defined by

$$\mathcal{D}^{\pm}_{i+\frac{1}{2}}(\mathbf{W}^-_{i+\frac{1}{2}}, \mathbf{W}^+_{i+\frac{1}{2}}) = \frac{1}{2}\int_0^1 \Big(\mathbf{J}(\Theta(s)) \pm |\mathbf{J}(\Theta(s))|\Big)\frac{d\Theta}{ds} ds, \tag{46}$$

with Θ a Liptschitzian path in $[0,1]$ satisfying

$$\Theta(0) = \mathbf{W}^-_{i+\frac{1}{2}}\,,\ \Theta(1) = \mathbf{W}^+_{i+\frac{1}{2}}.$$

For more details see [15, 49, 41] and references therein.

2.2 The Dumbser-Enaux-Toro (DET) solver for the GRP

Here the generalized Riemann problem is the following Cauchy problem

$$\left.\begin{aligned} \partial_t \mathbf{W} + \mathbf{J}\partial_x \mathbf{W} &= \mathbf{L}(\mathbf{W})\,, \\ \mathbf{W}(x,0) &= \begin{cases} \mathbf{P}_i(x)\,, x < x_{i+\frac{1}{2}}, \\ \mathbf{P}_{i+1}(x)\,, x > x_{i+\frac{1}{2}}, \end{cases} \end{aligned}\right\} \tag{47}$$

where $\mathbf{P}_i(x)$ and $\mathbf{P}_{i+1}(x)$ are reconstruction polynomials defined in I_i and I_{i+1} respectively. In this paper we use the WENO reconstruction procedure proposed in [42]. See also [33] and [20] for background on WENO reconstruction.

The solution of (47) allows us to approximate time integrals (45) with a required order of accuracy. Here we use the Dumbser-Enaux-Toro (DET) solver [21]. Data to the left and right of the interface $x_{i+\frac{1}{2}}$, necessary for the computation of numerical fluxes at quadrature points, are obtained by solving a local Cauchy problem in each element of the computational mesh. This solver yields $\mathbf{W}_i(x,t)$, that will be used to approximate integrals appearing in (44) by quadrature rules.

In the DET solver, we solve the local Cauchy problem in I_i^n, namely

$$\left.\begin{array}{rcl} \partial_t \mathbf{W} + \mathbf{J}\partial_x \mathbf{W} & = & \mathbf{L}(\mathbf{W}), \\ \mathbf{W}(x,0) & = & \mathbf{P}_i(x). \end{array}\right\} \tag{48}$$

We transform the space-time interval I_i^n into $[0,1]\times[0,1]$, with reference variables $\xi-\tau$ given by the change of variables $x = x(\xi) = x_{i-\frac{1}{2}} + \xi\Delta x$ and $t = t(\tau) = t^n + \tau\Delta t$. The problem in $\xi-\tau$ variables reads

$$\begin{array}{rcl} \partial_\tau \mathcal{W} + \mathfrak{J}\partial_\xi \mathcal{W} & = & \mathcal{L}(\mathcal{W}), \\ \mathcal{W}(\xi,0) & = & \mathbf{P}_i(x(\xi)), \end{array} \tag{49}$$

with $\mathfrak{J} = \frac{\Delta t}{\Delta x}\mathbf{J}$ and $\mathcal{L} = \Delta t\mathbf{L}$.

Problem (49) is now solved using a space-time discontinuous Galerkin method. Consider a space $\mathbf{V}$ formed by nodal space-time polynomials $\theta_p(\xi,\tau)$ defined in $[0,1]\times[0,1]$, whose basis is $\{\theta_1,...,\theta_m\}$. Here $m = (K+1)^2$, with K the degree of the reconstruction polynomials in (48) and $K+1$ the degrees of freedom of the space-time basis. Note that $K+1$ will also be the order of accuracy of the resulting ADER numerical scheme.

Multiplying (49) by a test function $\theta_l \in V$ and integrating in $[0,1]\times[0,1]$ we have

$$\int_0^1\int_0^1 \left[(\partial_\tau \mathcal{W})\theta_l + (\mathfrak{J}(\mathcal{W})\partial_\xi \mathcal{W})\theta_l\right] d\xi d\tau = \int_0^1\int_0^1 \mathcal{L}(\mathcal{W})\theta_l d\xi d\tau\,. \tag{50}$$

Integrating by parts in time τ the first term on the left hand side yields

$$\left.\begin{array}{l} \int_0^1\int_0^1 \partial_\tau \mathcal{W}(\xi,\tau)\theta_l(\xi,\tau)d\xi d\tau = \int_0^1 \mathcal{W}(\xi,1)\theta_l(\xi,1)d\xi \\ -\int_0^1 \mathbf{P}_i(x(\xi))\theta_l(\xi,0)d\xi - \int_0^1\int_0^1 \mathcal{W}(\xi,\tau)\partial_\tau\theta_l(\xi,\tau)d\xi d\tau\,. \end{array}\right\} \tag{51}$$

Substituting (51) into (50) gives

$$\left.\begin{array}{l} \int_0^1 \mathcal{W}(\xi,1)\theta_l(\xi,1) - \int_0^1\int_0^1 \mathcal{W}(\xi,\tau)\partial_\tau\theta_l(\xi,\tau)d\xi d\tau \\ +\int_0^1\int_0^1 \mathfrak{J}(\mathcal{W}(\xi,\tau))\partial_\xi \mathcal{W}(\xi,\tau)\theta_l(\xi,\tau)d\xi d\tau \\ = \int_0^1\int_0^1 \mathcal{L}(\mathcal{W}(\xi,\tau))\theta_l(\xi,\tau)d\xi d\tau + \int_0^1 \mathbf{P}_i(x(\xi))\theta_l(\xi,0)d\xi\,. \end{array}\right\} \tag{52}$$

We now introduce the following operators for any two functions $\phi(\xi,\tau)$ and $\psi(\xi,\tau)$, namely

$$\left[\phi,\psi\right]_\tau = \int_0^1 \phi(\xi,\tau)\psi(\xi,\tau)d\xi\,, \qquad \left\langle\phi,\psi\right\rangle = \int_0^1\int_0^1 \phi(\xi,\tau)\psi(\xi,\tau)d\xi d\tau\,. \tag{53}$$

Introducing these definitions into (52) yields

$$[\mathcal{W},\theta_l]_1 - \langle \mathcal{W},\partial_\tau\theta_l\rangle + \left\langle \mathfrak{J}(\mathcal{W})\partial_\xi \mathcal{W},\theta_l\right\rangle = \langle \mathcal{L}(\mathcal{W}),\theta_l\rangle + [\mathbf{P}_i,\theta_l]_0\,, \tag{54}$$

with

$$[\mathbf{P}_i,\theta_l]_0 = \int_0^1 \mathbf{P}_i(x(\xi))\theta_l(\xi,0)d\xi\,. \tag{55}$$

We seek solutions of the form

$$\mathcal{W}(\xi,\tau) = \textstyle\sum_{p=1}^m \theta_p(\xi,\tau)\hat{\mathcal{W}}_p\,, \tag{56}$$

with coefficients $\hat{\mathcal{W}}_k$ yet to be determined.

For convenience we define matrices

$$\left.\begin{aligned} \mathbf{K}^1_{k,l} &= [\theta_k,\theta_l]_1 - \langle \theta_k, \partial_\tau \theta_l \rangle \,, \\ \mathbf{K}^\xi_{k,l} &= \langle \partial_\xi \theta_k, \theta_l \rangle \,, \\ \mathbf{M}_{k,l} &= \langle \theta_k, \theta_l \rangle \,, \\ \mathbf{V}_{rec,l} &= [\mathbf{P}_i, \theta_l]_0 \,. \end{aligned}\right\} \tag{57}$$

On the other hand, as we are considering a nodal base, then

$$\mathfrak{J}(\mathcal{W})\partial_\xi \mathcal{W} = \mathfrak{J}\Big(\sum_{p=1}^{m} \theta_p(\xi,\tau)\hat{\mathcal{W}}_p\Big)\partial_\xi\Big(\sum_{p=1}^{m} \theta_p(\xi,\tau)\hat{\mathcal{W}}_p\Big) \approx \sum_{p=1}^{m} \partial_\xi\theta_p(\xi,\tau)\mathfrak{J}(\hat{\mathcal{W}}_p)\hat{\mathcal{W}}_p = \sum_{p=1}^{m} \theta_p(\xi,\tau)\hat{\mathcal{X}}_p \,. \tag{58}$$

with $\hat{\mathcal{X}}_p$ coefficients directly computed on the polynomial space $\mathbf{V}$, *i. e.* solving

$$\mathbf{X} = \mathbf{M}^{-1}\mathbf{K}^\xi \mathbf{JW} \,, \tag{59}$$

with $\mathbf{X} = \left[\hat{\mathcal{X}}_1,...,\hat{\mathcal{X}}_m\right]^T$ and $\mathbf{JW} = \left[\mathfrak{J}(\hat{\mathcal{W}}_1)\hat{\mathcal{W}}_1,...,\mathfrak{J}(\hat{\mathcal{W}}_m)\hat{\mathcal{W}}_m\right]^T$. In the same manner by projection on the polynomial space we obtain

$$\mathcal{L}(\mathcal{W}) \quad \approx \quad \textstyle\sum_{p=1}^{m} \theta_p(\xi,\tau)\mathcal{L}(\hat{\mathcal{W}}_p) \,. \tag{60}$$

Note that $\hat{\mathcal{X}}$ depends on coefficients $\hat{\mathcal{W}}$ so that we can define the vectors

$$\mathcal{R} = \begin{bmatrix} \hat{\mathcal{W}}_1 \\ \vdots \\ \hat{\mathcal{W}}_m \end{bmatrix}, \quad \mathcal{G}(\mathcal{R}) = \begin{bmatrix} \hat{\mathcal{X}}_1(\mathcal{R}) \\ \vdots \\ \hat{\mathcal{X}}_m(\mathcal{R}) \end{bmatrix}, \quad \mathcal{Z}(\mathcal{R}) = \begin{bmatrix} \mathcal{L}(\hat{\mathcal{W}}_1) \\ \vdots \\ \mathcal{L}(\hat{\mathcal{W}}_m) \end{bmatrix}. \tag{61}$$

Then, (54) can be written as

$$\mathbf{K}^1\mathcal{R} + \mathbf{M}\mathcal{G}(\mathcal{R}) - \mathbf{M}\mathcal{Z}(\mathcal{R}) = \mathbf{V}_{rec} \,. \tag{62}$$

This is a system of non-linear algebraic equations for $\mathcal{R}$ which can be solved by the fixed point iteration procedure proposed in [19], namely

$$\mathbf{K}^1\mathcal{R}^{n+1} - \mathbf{M}\mathcal{Z}(\mathcal{R}^{n+1}) = \mathbf{V}_{rec} - \mathbf{M}\mathcal{G}(\mathcal{R}^n), \tag{63}$$

where n stands for the iteration step. Once $\mathcal{R}$ is known, the sought coefficients are known and so the solution (56). We denote the solution to (49) by $\mathcal{W}_i(\xi,\tau)$ to clarify that it corresponds to the solution of the Cauchy problem in I_i^n.

Once that $\mathcal{W}_i(\xi,\tau)$ is available in all computational cells, integrals in (44) can be approximated by evaluating $\mathcal{W}_i(\xi,\tau)$ in selected quadrature points. Moreover, numerical fluctuations appearing in time integrals in (45) are obtained by using a first order classical Riemann solver at required quadrature points τ_k with $\mathcal{W}_i(1,\tau_k)$ and $\mathcal{W}_{i+1}(0,\tau_k)$. In the following section we introduce the first order Riemann solver used in the present work.

2.3 The Dumbser-Osher-Toro (DOT) Riemann solver: Fluctuations

To compute fluctuations we will use the DOT solver of Dumbser and Toro [25]. Let $\lambda_i(\mathbf{W})$ be the $i-th$ eigenvalue of $\mathbf{J}(\mathbf{W})$, then $\Lambda(\mathbf{W})$ is the matrix formed by all eigenvalues $\lambda_i(\mathbf{W})$, and let $\mathbf{R}(\mathbf{W})$ be the matrix formed by the right eigenvectors of $\mathbf{J}(\mathbf{W})$. We define

$$\lambda_i(\mathbf{W})^+ = max\{\lambda_i(\mathbf{W}),0\} \quad , \quad \lambda_i(\mathbf{W})^- = min\{\lambda_i(\mathbf{W}),0\}\,. \tag{64}$$

Let $\Lambda(\mathbf{W})^+$ be the diagonal matrix formed by $\lambda_i(\mathbf{W})^+$ and let $\Lambda(\mathbf{W})^-$ be the diagonal matrix formed by $\lambda_i(\mathbf{W})^-$. Then, we define the matrices $|\Lambda|$ and $|\mathbf{J}|$ by

$$|\Lambda(\mathbf{W})| = \Lambda(\mathbf{W})^+ - \Lambda(\mathbf{W})^- \tag{65}$$

and

$$|\mathbf{J}(\mathbf{W})| = \mathbf{R}(\mathbf{W})|\Lambda(\mathbf{W})|\mathbf{R}(\mathbf{W})^{-1}\,. \tag{66}$$

Let us consider the interface $x_{i+\frac{1}{2}}$ where data on the left is denoted by $\mathbf{W}_L$ and data on the right is denoted by $\mathbf{W}_R$. The fluctuation at the interface is computed as

$$\mathcal{D}^{\pm}_{i+\frac{1}{2}}(\mathbf{W}_L,\mathbf{W}_R) = \frac{1}{2}\int_0^1 \Big(\mathbf{J}(\Theta(s)) \pm |\mathbf{J}(\Theta(s))|\Big)\frac{\partial \Theta}{\partial s} ds\,, \tag{67}$$

where the integral is evaluated numerically. We consider a Gaussian quadrature of n points and weights $\{\omega_j, s_j\}$.

We still have to define the integration path Θ. If we choose the path

$$\Theta(s) = \mathbf{W}_L + s\,(\mathbf{W}_R - \mathbf{W}_L)\,, \tag{68}$$

the fluctuations are

$$\mathcal{D}^{\pm}_{i+\frac{1}{2}}(\mathbf{W}_L,\mathbf{W}_R) = \frac{1}{2}\sum_{j=1}^{n} \omega_j \Big(\mathbf{J}(\Theta(s_j)) \pm |\mathbf{J}(\Theta(s_j))|\Big)(\mathbf{W}_R - \mathbf{W}_L)\,. \tag{69}$$

However, in order to preserve and guarantee well-balanced properties, the integration path $\Theta(s)$ should be chosen as the parametrization in phase-space of the curve $\mathfrak{L}^1$ in proposition 1.5, defined by the Riemann invariants associated to linearly-degenerate fields as proposed by Müller *et al.* [41, 42]. In the next subsection we illustrate how path Θ is constructed.

2.4 Integration path

As proposed in [42], to guarantee well-balanced properties we take the integration path as

$$\Theta(s) = \begin{bmatrix} A(s) \\ q(s) = q^-_{i+\frac{1}{2}} + s\Big(q^+_{i+\frac{1}{2}} - q^-_{i+\frac{1}{2}}\Big) \\ K(s) = K^-_{i+\frac{1}{2}} + s\Big(K^+_{i+\frac{1}{2}} - K^-_{i+\frac{1}{2}}\Big) \\ A_0(s) = A^-_{0,i+\frac{1}{2}} + s\Big(A^+_{0,i+\frac{1}{2}} - A^-_{0,i+\frac{1}{2}}\Big) \\ p_e(s) = p^-_{e,i+\frac{1}{2}} + s\Big(p^+_{e,i+\frac{1}{2}} - p^-_{e,i+\frac{1}{2}}\Big) \\ \Psi(s) = \Psi^-_{i+\frac{1}{2}} + s\Big(\Psi^+_{i+\frac{1}{2}} - \Psi^-_{i+\frac{1}{2}}\Big) \end{bmatrix}, \tag{70}$$

where super index − refers to the data immediately to the left of the interface and super index + refers to the data immediately to the right of the interface. $A(s)$ is obtained from the arch joining two states $A^-_{i+\frac{1}{2}}$ and $A^+_{i+\frac{1}{2}}$, through the curve defined by Riemann invariants $\mathfrak{L}^1$ of the linearly degenerated field. To determine this curve, we first note that for the stationary state case, $q = 0$, we have

$$\mathfrak{L}^1(A, A_0, K, p_e) = K\phi(A, A_0) + p_e \,. \tag{71}$$

Therefore, $A(s)$ can be obtained from the algebraic equation

$$\phi(A(s), A_0(s)) = \frac{\bar{\mathfrak{L}}^1(s) - p_e(s)}{K(s)} \,,$$

with

$$\bar{\mathfrak{L}}^1(s) = (1-s)\,\mathfrak{L}^1(A^-_{i+\frac{1}{2}}, A^-_{0,i+\frac{1}{2}}, K^-_{i+\frac{1}{2}}, p^-_{e,i+\frac{1}{2}}) + s\,\mathfrak{L}^1(A^+_{i+\frac{1}{2}}, A^+_{0,i+\frac{1}{2}}, K^+_{i+\frac{1}{2}}, p^+_{e,i+\frac{1}{2}}) \,. \tag{72}$$

Finally, we define the time step at time t^n as

$$\Delta t = C_{cfl}\frac{\Delta x}{\lambda_{max}} \,, \tag{73}$$

where $\lambda_{max} = max_{i=1,\dots,m}|\lambda_i(\mathbf{W}^n)|$ and $\mathbf{W}^n$ is the corresponding data evaluated at time t^n.

3 Numerical accuracy of solutions to ADR equations by hyperbolic reformulation

In order to solve numerically ADR problems, we reformulate them as hyperbolic systems with stiff source terms. Subsequently, we implement a numerical scheme which solves the stiff hyperbolic problem with order of accuracy q. However, it is desirable that the numerical solution approximates the solution to the original ADR problem with the same order of accuracy q. In this section we present a result of sufficiency which ensures this property. This result is independent of the specific ADR problem and depends only on the relaxation time ε, the convergence rate q and the mesh spacing Δx. Furthermore, we provide numerical evidence that supports this result.

3.1 A sufficiency criterion for ensuring theoretically expected accuracy

From Nagy *et al.* [44] the solution of the hyperbolized problem, u_h, and the solution of the original ADR problem, u_p, are related by

$$u_p = u_h + O(\varepsilon) \,, \tag{74}$$

where $O(\varepsilon)$ represents the formulation error in the relaxation approach. If we consider a numerical scheme able to solve a hyperbolic problem with an accuracy of order q, then, taking into account (73), we can write

$$\tilde{u} = u_h + O(\Delta x^q) \,, \tag{75}$$

where $\tilde{u}$ represents the numerical solution and Δx is the mesh size. Thus $O(\Delta x^q)$ represents the numerical error for the hyperbolic problem. The following result summarizes a sufficiency condition which guarantees that the ADR problem is solved with accuracy q.

Proposition 3.1. *The solution of the ADR problem (1) by means of the hyperbolic reformulation (6), is approximated with accuracy q for all ε and Δx satisfying*

$$\triangle := \frac{\varepsilon}{(\Delta x)^q} K_q = O(1)\,, \tag{76}$$

where

$$K_q = \frac{1-2^{-\frac{1}{2}}}{2^{q-\frac{1}{2}}-1}\,.$$

Proof. From (74) and (75) we obtain

$$\tilde{u} - u_p = u_h - u_p + O(\Delta x^q)\,, \tag{77}$$

which allows us to relate the formulation error and the numerical error as

$$O(\Delta x^r) = O(\varepsilon) + O(\Delta x^q)\,, \tag{78}$$

where r is the order of accuracy by which the numerical scheme approximates the solution of original ADR problem. Note that the numerical error can be expressed as

$$O(\Delta x^r) = C\Delta x^r\,, \tag{79}$$

with C depending on the problem to be solved, but is independent of the mesh spacing Δx.

We denote by $\tilde{u}_k$ the numerical solution obtained with a mesh of length Δx_k. Therefore, from (78) and (79), on two successive meshes with lengths Δx_k, Δx_{k+1}, we obtain

$$\left(\frac{\Delta x_k}{\Delta x_{k+1}}\right)^r = \frac{O(\varepsilon) + O(\Delta x_k^q)}{O(\varepsilon) + O(\Delta x_{k+1}^q)}\,, \tag{80}$$

yielding after manipulations

$$\left(\frac{\Delta x_k}{\Delta x_{k+1}}\right)^r = \left(\frac{\Delta x_k}{\Delta x_{k+1}}\right)^q \theta\,, \tag{81}$$

with

$$\theta = \frac{\frac{O(\varepsilon)}{O(\Delta x_k^q)} + O(1)}{\frac{O(\varepsilon)}{O(\Delta x_{k+1}^q)} + O(1)}\,. \tag{82}$$

Without loss of generality, we assume $\Delta x_k = 2\Delta x_{k+1}$. Taking logarithm in (81), we obtain

$$r = q + \log(\theta)/\log(2)\,. \tag{83}$$

Let us now assume that given an expected order of accuracy q, we consider that the numerical scheme yields this accuracy if

$$r \geq q - \frac{1}{2}\,.$$

Therefore, the order of accuracy for the ADR problem attains that of the hyperbolic problem when

$$-\tfrac{1}{2} < \log(\theta)/\log(2)\,. \tag{84}$$

From the monotonicity of the logarithm, (84) is equivalent to

$$\frac{1}{\sqrt{2}} < \theta \,, \tag{85}$$

which yields

$$\frac{1}{\sqrt{2}}\left(2^q \frac{O(\varepsilon)}{O(\Delta x_k^q)} + O(1)\right) < \frac{O(\varepsilon)}{O(\Delta x_k^q)} + O(1) \,, \tag{86}$$

or

$$\frac{O(\varepsilon)}{O(\Delta x_k^q)} < O(1)\left(\frac{1-2^{-\frac{1}{2}}}{2^{q-\frac{1}{2}}-1}\right). \tag{87}$$

Moreover, we assume that

$$\frac{O(\varepsilon)}{O(\Delta x_k^q)} = O\left(\frac{\varepsilon}{\Delta x_k^q}\right) = K\frac{\varepsilon}{\Delta x_k^q} \,, \tag{88}$$

with K to be determined. Therefore, we impose that

$$K\frac{\varepsilon}{\Delta x_k^q} = O(1) \,, \tag{89}$$

or

$$K\varepsilon 2^{\bar{n}q} = O(1) \,, \tag{90}$$

noting that it is possible to set $\Delta x = 2^{-\bar{n}}$, where $\bar{n} = \log_2(1/\Delta x)$. So, inspired by (87), for all $\bar{n} \geq 0$ we set

$$K\varepsilon \leq \frac{1}{2^{\bar{n}q}}\left(\frac{1-2^{-\frac{1}{2}}}{2^{q-\frac{1}{2}}-1}\right) \leq \left(\frac{1-2^{-\frac{1}{2}}}{2^{q-\frac{1}{2}}-1}\right). \tag{91}$$

For convenience we take $K \leq \varepsilon^{-1}K_{max}$, as to maintain order $O(1)$. Thus, we have

$$K_{max} := \varepsilon\frac{1-2^{-\frac{1}{2}}}{2^{q-\frac{1}{2}}-1} \,. \tag{92}$$

In this manner, a sufficiency condition to maintain accuracy solving the ADR problem for a given mesh of size Δx is given by

$$\frac{\varepsilon}{(\Delta x)^q}K_q = O(1) \,, \tag{93}$$

where $K_q = \varepsilon^{-1}K_{max}$.

□

Remark 3.2. *Note that if in equation (76) the left-hand side is greater than $O(1)$, the formulation error dominates over the numerical one. From the right hand side in (78), a mesh refinement reduces the numerical error whereas the formulation error remains, becoming the barrier for the accuracy of the numerical scheme.*

Remark 3.3. *In this work we assume $O(1) = 15$, which is the sum of the maximum magnitude accepted as $O(1)$, plus its rounding error. We observe that given a relaxation parameter ε it is possible to predict the maximum number of cells such that the sought accuracy is attained.*

3.2 Convergence rate study for an ADR problem via hyperbolic reformulation

Here, we provide numerical results that confirm proposition 3.1 for the particular case of the one-dimensional blood flow model (16). To assess empirically the accuracy of the high-order numerical scheme (44) and the ability of reformulation (20) to recover the solution of the original viscoelastic problem (16), we construct a modified problem with exact solution. This is achieved by prescribing a function to be inserted in (16). Here we choose such function as

$$\hat{\mathbf{Q}}(x,t) = \begin{bmatrix} \hat{A}(x,t) \\ \hat{q}(x,t) \\ \hat{K}(x) \\ \hat{A}_0(x) \\ \hat{p}_e(x) \end{bmatrix} = \begin{bmatrix} \tilde{A} + \tilde{a}\, sin\left(\frac{2\pi}{L}x\right) cos\left(\frac{2\pi}{T_0}t\right) \\ \tilde{q} - \tilde{a}\,\frac{L}{T_0}\, cos\left(\frac{2\pi}{L}x\right) sin\left(\frac{2\pi}{T_0}t\right) \\ \tilde{K} \\ \tilde{A}_0 \\ \tilde{P}_e \end{bmatrix}. \tag{94}$$

Inserting (94) in (16) leads to the modified system

$$\partial_t \mathbf{Q} + \mathbf{A}(\mathbf{Q})\partial_x \mathbf{Q} = \partial_x \mathbf{G}(\mathbf{Q}, \partial_x \mathbf{Q}) + \mathbf{S}(\mathbf{Q}) + \hat{\mathbf{S}}(x,t), \tag{95}$$

where $\hat{\mathbf{S}}(x,t)$ results from the evaluation of (94) in (16) and is only a function of time t and space x variables. $\hat{\mathbf{S}}(x,t)$ may be found with an algebraic manipulator and is not reported here. For the present study we use the following parameters: $L = 1.0\,m$, $T_0 = 1.0\,s$, $\tilde{A} = \tilde{A}_0 = 4.0 \times 10^{-4}\,m^2$, $\tilde{a} = 4.0 \times 10^{-5}\,m^2$, $\tilde{q} = 0.0\,m^3\,s^{-1}$, $\tilde{K} = 50.0\,KPa$, $\tilde{P}_e = 0.0\,Pa$, $m = 1/2$ and $n = 0$. For this test we used a $CFL = 0.9$.

Tables 1 to 4 show the empirical convergence rates from second to fifth order ADER schemes with several relaxation times ε. The highlighted row corresponds to the largest number of cells N for which, according to proposition 3.1, the theoretical convergence rate is expected to be achieved. It can be seen that the expected empirical accuracy is achieved for all orders of accuracy, and at least up to the predicted maximum number of cells.

Another interesting aspect to be noted is that when the discretization error becomes smaller than the formulation error, the error norms become independent from further mesh refinement, as expected.

4 Computational results for a network of viscoelastic vessels

In this section we validate our numerical scheme in the context of an *in-vitro* model of the human arterial system.

4.1 Review of reference *in-vitro* model of the arterial system

An *in-vitro* model of the human arterial system was put forward by Matthys *et al.* [39]. Along with an accurate description of the physical model, the authors constructed the corresponding mathematical model for one-dimensional blood flow in elastic vessels and provided a wealth of measurements and numerical results. The vessel network is composed of 37 silicone tubes resembling major arteries, a pump acting as the heart and terminal resistances representing the peripheral circulation. We refer the reader to the above named reference for details on the topography of the network, the description of mechanical properties, geometry of the vessels, terminal resistances and flow rate measured at the root of the ascending aorta. In a subsequent publication,

Alastruey *et al.* [2], a viscoelastic vessel wall model was used in order to improve computational results for specific portions of the network, where non-physical high amplitude oscillation were observed. This test constitutes an ideal benchmark for assessing the performance of the methodology proposed in this paper in the context of a complex network of viscoelastic vessels.

4.2 Details on the settings of the network solver

Modelling the network of vessels proposed in [39] requires dealing with other aspects besides the solution of system (16) within the one-dimensional domain. In particular, the flow rate has to be prescribed at the root of the aorta, terminal lumped parameter models have to be resolved and interface conditions at the junction between two or more vessels have to be given. Boundary conditions involving a prescribed flow rate or terminal resistances were treated as in [4]. For the treatment of junctions, the methodology proposed in [53] was used. Details on the treatment of boundary conditions and junctions are given in A.

We adopted the spatial discretisation of [2]: vessels longer than 1.5 cm were divided in non-overlapping cells of a maximum length of 2 cm; for vessels shorter than 1.5 cm a single cell was used. Taking into account the results of proposition 3.1 and the fact that the characteristic mesh spacing is of order $\Delta x = 2\,cm$ for almost all vessels, we used a relaxation time $\epsilon = 10^{-3}\,s$ over the entire network. This choice ensures that the formulation error will be smaller than the numerical error for all vessels, except for 3 vessels which would require a relaxation time of $\epsilon = 10^{-4}\,s$. As we shall see later, this choice will not have a significant impact on the numerical results.

Computations were performed using a $CFL = 0.9$, which combined with the chosen relaxation time results in an average time step of approximately $\Delta t = 400\,\mu s$. Note that the time step Δt is computed at each time step, in order to advance as much as possible in time during each step, within the linear stability limit of unity of our explicit scheme.

4.3 Comparison of solutions obtained using elastic and viscoelastic vessel wall models

Our first validation regards a comparison among experimental measurements reported in [2], numerical results for elastic vessels reported in [42] and numerical results for the viscoelastic model (16) obtained with the methodology presented in section 2 of this paper. We note that the one-dimensional model for elastic vessels results from taking $\Gamma = 0$ in (13).

Figure 1 shows experimental measurements and computational results for both the elastic and viscoelastic vessel wall models. It can be easily seen that the solution obtained with the elastic model presents abnormally large amplitude fluctuations, as compared to experiments, in the left renal and right carotid arteries during diastole. This phenomenon can be observed for both measured quantities, pressure and flow rate, being more evident for the later one. The viscoelastic formulation significantly increases the accuracy by which the numerical solution approximates experimental measurements, reducing non-physical oscillations for pressure and flow rate.

4.4 Comparison with published numerical results

Here, we compare numerical results obtained with the proposed formulation and numerical results previously reported in [2]. Figure 2 shows both numerical results, along with experimental measurements for several vessels. Agreement between numerical results obtained with the proposed methodology and those reported in [2] is excellent. We note that the time step of our explicit scheme is around 20 times larger than that in [2], where a time step of $\Delta t = 20\,\mu s$ was reported.

4.5 Sensitivity of the numerical solution to the relaxation time ε

In figure 3 we report numerical results for different relaxation times ε. As expected, there is a significant difference between results obtained using $\varepsilon = 10^{-2}\,s$ and $\varepsilon = 10^{-3}\,s$ for vessels which show high frequency oscillations (right carotid artery). This is due to the fact that in the first case the formulation error dominates over the discretization error, whereas for $\varepsilon = 10^{-3}\,s$ we are attaining the expected accuracy of the numerical scheme for almost all vessels. Further reduction of ε does not result in significant improvement of the numerical solution, since the discretization error remains dominant. Finally, the last row of figure 3 shows computational results for the shortest vessel of the network, which would require a relaxation time $\varepsilon = 10^{-4}\,s$. Improvements with respect to the numerical solution obtained using $\varepsilon = 10^{-3}\,s$ are negligible.

5 Conclusions

In this paper we have reformulated a one-dimensional blood flow model for viscoelastic vessels in the form of a hyperbolic system with stiff source terms, via a relaxation approach. After carefully studying the mathematical properties of the resulting system we proposed a methodology for its numerical solution, ensuring high-order accuracy and well-balanced properties. Next, we defined a criterion for selecting the relaxation time which depends only on the order of accuracy of the numerical scheme used to solve the hyperbolic system and the mesh spacing. This criterion ensures that the formulation error will be smaller than the discretisation error. Moreover, the order of accuracy of the numerical scheme, as well as the proposed criterion for the definition of the relaxation time, were tested via an empirical convergence rate study up to fifth order of accuracy in space and time. Empirical results confirm the theory. Finally, we validated the proposed methodology by comparing our numerical results with experimental measurements, as well as with numerical results reported in the literature for a network of viscoelastic vessels. We showed that: the viscoelastic formulation improves the agreement between numerical results and experimental measurements, as compared to the results obtained considering elastic vessels; numerical results obtained with the proposed methodology are in agreement with previously reported data. The choice of the relaxation time via the proposed criterion ensures an accurate numerical solution, also in the context of complex vessel networks.

Acknowledgements

The authors warmly thank Dr. Jordy Alastruey (King's College and St Thomas' Hospital, London, UK) for providing experimental measurements and numerical results reported in [2].

This work has been partially funded by CARITRO (*Fondazione Cassa di Risparmio di Trento e Rovereto*, Italy), project No. 2011.0214.

ADER-O2

ε	N	L^1	L^2	L^∞	$\mathcal{O}(L^1)$	$\mathcal{O}(L^2)$	$\mathcal{O}(L^\infty)$	$t_{CPU}\,[s]$	$\triangle$
10^{-2}	4	1.08e-05	1.23e-05	2.46e-05	-	-	-	0.59	
	8	2.58e-06	3.02e-06	7.42e-06	2.1	2.0	1.7	0.92	1.03e-01
	16	5.58e-07	7.01e-07	2.11e-06	2.2	2.1	1.8	1.90	4.10e-01
	32	1.34e-07	1.70e-07	5.24e-07	2.1	2.0	2.0	4.49	1.64e+00
	64	3.50e-08	4.34e-08	1.19e-07	1.9	2.0	2.1	10.14	6.52e+00
	128	1.48e-08	1.87e-08	4.18e-08	1.2	1.2	1.5	25.22	2.62e+01
10^{-3}	4	1.05e-05	1.27e-05	2.86e-05	-	-	-	0.89	
	8	2.34e-06	3.07e-06	9.24e-06	2.2	2.0	1.6	1.17	1.03e-02
	16	5.39e-07	7.45e-07	2.45e-06	2.1	2.0	1.9	3.81	4.10e-02
	32	1.30e-07	1.83e-07	6.17e-07	2.1	2.0	2.0	8.10	1.64e-01
	64	3.17e-08	4.50e-08	1.55e-07	2.0	2.0	2.0	16.23	6.58e-01
	128	7.79e-09	1.08e-08	3.76e-08	2.0	2.1	2.0	39.74	2.62e+00
	256	2.06e-09	2.59e-09	7.64e-09	1.9	2.1	2.3	92.13	1.05e+01
	512	1.26e-09	1.53e-09	3.05e-09	0.7	0.8	1.3	276.16	4.20e+01
10^{-4}	4	1.14e-05	1.28e-05	2.18e-05	-	-	-	2.25	
	8	2.26e-06	3.29e-06	1.04e-05	2.3	2.0	1.1	2.32	1.03e-03
	16	5.65e-07	8.54e-07	2.82e-06	2.0	1.9	1.9	8.09	4.10e-03
	32	1.36e-07	2.03e-07	6.85e-07	2.1	2.1	2.0	21.26	1.64e-02
	64	3.31e-08	4.96e-08	1.69e-07	2.0	2.0	2.0	42.51	6.56e-02
	128	8.20e-09	1.23e-08	4.23e-08	2.0	2.0	2.0	89.87	2.62e-01
	256	2.02e-09	3.02e-09	1.04e-08	2.0	2.0	2.0	234.33	1.05e-00
	512	4.85e-10	6.96e-10	2.43e-09	2.1	2.1	2.1	738.74	4.20e+00
	1024	1.37e-10	1.69e-10	4.27e-10	1.8	2.0	2.5	2501.83	1.68e+01
	2048	1.29e-10	1.48e-10	2.70e-10	0.1	0.2	0.7	8757.74	6.72e+01
10^{-5}	4	1.95e-05	2.25e-05	3.33e-05	-	-	-	5.40	
	8	5.75e-06	6.97e-06	1.45e-05	1.8	1.7	1.2	9.50	1.03e-04
	16	1.04e-06	1.40e-06	3.40e-06	2.5	2.3	2.1	27.35	4.10e-04
	32	1.83e-07	2.57e-07	7.60e-07	2.5	2.4	2.2	59.42	1.64e-03
	64	3.74e-08	5.51e-08	1.81e-07	2.3	2.2	2.1	128.79	6.56e-03
	128	8.76e-09	1.33e-08	4.48e-08	2.1	2.1	2.0	279.25	2.62e-02
	256	2.15e-09	3.29e-09	1.12e-08	2.0	2.0	2.0	745.23	1.05e-01
	512	5.33e-10	8.17e-10	2.78e-09	2.0	2.0	2.0	2210.56	4.20e-01
	1024	1.29e-10	1.97e-10	6.78e-10	2.0	2.1	2.0	7216.78	1.68e+00
	2048	3.03e-11	4.30e-11	1.51e-10	2.1	2.2	2.2	25564.93	6.72e+00
	4096	1.07e-11	1.32e-11	2.78e-11	1.5	1.7	2.4	96751.62	2.69e+01

Table 1: Empirical convergence rates for a second order ADER scheme with several relaxation times ε. N is the number of cells. Errors are computed for variable A. CPU times are reported for all tests. The highlighted row corresponds to the largest number of cells N for which, predicted by proposition 3.1, the theoretical convergence rate is expected to be achieved.

ADER-O3

ε	N	L^1	L^2	L^∞	$\mathcal{O}(L^1)$	$\mathcal{O}(L^2)$	$\mathcal{O}(L^\infty)$	$t_{CPU}[s]$	$\triangle$
10^{-2}	4	4.31e-06	4.85e-06	8.38e-06	-	-	-	0.70	
	8	5.91e-07	7.16e-07	1.46e-06	2.9	2.8	2.5	1.34	3.22e-01
	16	7.43e-08	9.18e-08	2.03e-07	3.0	3.0	2.8	2.70	2.58e+00
	32	1.84e-08	2.07e-08	3.57e-08	2.0	2.2	2.5	5.54	2.06e+01
	64	1.54e-08	1.71e-08	2.52e-08	0.3	0.3	0.5	15.93	1.65e+02
10^{-3}	4	3.82e-06	4.59e-06	9.08e-06	-	-	-	0.94	
	8	5.46e-07	6.77e-07	1.47e-06	2.8	2.8	2.6	2.07	3.22e-02
	16	7.17e-08	8.94e-08	2.00e-07	2.9	2.9	2.9	4.14	2.58e-01
	32	9.06e-09	1.13e-08	2.60e-08	3.0	3.0	2.9	9.25	2.06e+00
	64	1.91e-09	2.16e-09	4.03e-09	2.2	2.4	2.7	24.20	1.65e+01
10^{-4}	4	3.82e-06	4.59e-06	9.10e-06	-	-	-	1.83	
	8	5.58e-07	6.90e-07	1.48e-06	2.8	2.7	2.6	5.14	3.22e-03
	16	7.35e-08	9.03e-08	1.99e-07	2.9	2.9	2.9	10.32	2.58e-02
	32	9.22e-09	1.14e-08	2.59e-08	3.0	3.0	2.9	25.53	2.06e-01
	64	1.15e-09	1.43e-09	3.39e-09	3.0	3.0	2.9	61.13	1.65e+00
	128	2.05e-10	2.37e-10	4.91e-10	2.5	2.6	2.8	161.16	1.32e+01
	256	1.53e-10	1.71e-10	2.65e-10	0.4	0.5	0.9	488.69	1.06e+02
10^{-5}	4	7.92e-06	9.24e-06	1.46e-05	-	-	-	6.21	
	8	5.75e-07	7.01e-07	1.49e-06	3.8	3.7	3.3	14.84	3.22e-04
	16	7.24e-08	8.98e-08	2.00e-07	3.0	3.0	2.9	32.91	2.58e-03
	32	9.58e-09	1.16e-08	2.59e-08	2.9	2.9	3.0	70.57	2.06e-02
	64	1.20e-09	1.47e-09	3.40e-09	3.0	3.0	2.9	175.85	1.65e-01
	128	1.50e-10	1.84e-10	4.54e-10	3.0	3.0	2.9	491.91	1.32e+00
	256	2.25e-11	2.72e-11	6.47e-11	2.7	2.8	2.8	1674.83	1.06e+01
	512	1.50e-11	1.68e-11	2.90e-11	0.6	0.7	1.2	4963.15	8.44e+01

Table 2: Empirical convergence rates for a third order ADER scheme with several relaxation times ε. N is the number of cells. Errors are computed for variable A. CPU times are reported for all tests. The highlighted row corresponds to the largest number of cells N for which, according to proposition 3.1, the theoretical convergence rate is expected to be achieved.

ADER-O4

ε	N	L^1	L^2	L^∞	$\mathcal{O}(L^1)$	$\mathcal{O}(L^2)$	$\mathcal{O}(L^\infty)$	$t_{CPU}\,[s]$	$\triangle$
10^{-2}	4	6.73e-06	7.68e-06	1.64e-05	-	-	-	0.81	
	8	3.94e-07	4.83e-07	1.21e-06	4.1	4.0	3.8	1.62	1.16e+00
	16	2.18e-08	2.47e-08	5.65e-08	4.2	4.3	4.4	3.66	1.86e+01
	32	1.49e-08	1.65e-08	2.55e-08	0.6	0.6	1.1	10.42	2.98e+02
10^{-3}	4	5.91e-06	7.80e-06	1.89e-05	-	-	-	1.11	
	8	4.94e-07	6.09e-07	1.55e-06	3.6	3.7	3.6	2.52	1.16e-01
	16	2.80e-08	3.56e-08	9.79e-08	4.1	4.1	4.0	6.02	1.86e+00
	32	9.59e-10	1.22e-09	4.02e-09	4.9	4.9	4.6	16.06	2.98e+01
	64	1.44e-09	1.60e-09	2.44e-09	-0.6	-0.4	0.7	40.93	4.76e+02
10^{-4}	4	6.27e-06	7.49e-06	1.74e-05	-	-	-	2.43	
	8	6.80e-07	8.16e-07	1.85e-06	3.2	3.2	3.2	6.32	1.16e-02
	16	4.00e-08	4.78e-08	1.18e-07	4.1	4.1	4.0	15.28	1.86e-01
	32	2.29e-09	2.77e-09	7.21e-09	4.1	4.1	4.0	39.87	2.98e+00
	64	5.79e-11	7.43e-11	2.61e-10	5.3	5.2	4.8	107.24	4.76e+01
	128	1.44e-10	1.61e-10	2.55e-10	-1.3	-1.1	0.0	335.48	7.62e+02
10^{-5}	4	1.57e-05	1.81e-05	2.64e-05	-	-	-	8.23	
	8	5.50e-07	6.73e-07	1.66e-06	4.8	4.7	4.0	18.71	1.16e-03
	16	4.53e-08	5.33e-08	1.26e-07	3.6	3.7	3.7	44.81	1.86e-02
	32	2.64e-09	3.12e-09	7.74e-09	4.1	4.1	4.0	113.75	2.98e-01
	64	1.46e-10	1.78e-10	4.89e-10	4.2	4.1	4.0	344.79	4.76e+00
	128	2.06e-11	2.24e-11	4.12e-11	2.8	3.0	3.6	1068.13	7.62e+01

Table 3: Empirical convergence rates for a fourth order ADER scheme with several relaxation times ε. N is the number of cells. Errors are computed for variable A. CPU times are reported for all tests. The highlighted row corresponds to the largest number of cells N for which, according to proposition 3.1, the theoretical convergence rate is expected to be achieved.

ADER-O5

ε	N	L^1	L^2	L^∞	$\mathcal{O}(L^1)$	$\mathcal{O}(L^2)$	$\mathcal{O}(L^\infty)$	$t_{CPU}\,[s]$	$\triangle$
10^{-2}	4	1.88e-06	2.10e-06	3.37e-06	-	-	-	1.08	
	8	7.88e-08	9.43e-08	1.90e-07	4.6	4.5	4.1	2.60	4.44e+00
	16	1.58e-08	1.75e-08	2.57e-08	2.3	2.4	2.9	6.75	1.42e+02
	32	1.54e-08	1.71e-08	2.47e-08	0.0	0.0	0.1	19.59	4.54e+03
10^{-3}	4	1.61e-06	1.88e-06	3.48e-06	-	-	-	1.32	
	8	6.71e-08	8.22e-08	1.71e-07	4.6	4.5	4.3	3.80	4.44e-01
	16	2.71e-09	3.21e-09	6.61e-09	4.6	4.7	4.7	10.52	1.42e+01
	32	1.54e-09	1.72e-09	2.49e-09	0.8	0.9	1.4	29.37	4.54e+02
10^{-4}	4	1.57e-06	1.94e-06	3.55e-06	-	-	-	3.51	
	8	6.90e-08	8.41e-08	1.73e-07	4.5	4.5	4.4	9.45	4.44e-02
	16	2.29e-09	2.83e-09	6.02e-09	4.9	4.9	4.8	25.46	1.42e+00
	32	1.66e-10	1.86e-10	3.08e-10	3.8	3.9	4.3	77.60	4.54e+01
10^{-5}	4	2.00e-06	2.24e-06	3.34e-06	-	-	-	10.37	
	8	6.93e-08	8.44e-08	1.74e-07	4.8	4.7	4.3	27.91	4.44e-03
	16	2.46e-09	2.92e-09	6.00e-09	4.8	4.9	4.9	78.60	1.42e-01
	32	7.24e-11	9.00e-11	1.95e-10	5.1	5.0	4.9	215.37	4.54e+00
	64	1.71e-11	1.90e-11	3.01e-11	2.1	2.2	2.7	724.42	1.54e+02

Table 4: Empirical convergence rates for a fifth order ADER scheme with several relaxation times ε. N is the number of cells. Errors are computed for variable A. CPU times are reported for all tests. The highlighted row corresponds to the largest number of cells N for which, according to proposition 3.1, the theoretical convergence rate is expected to be achieved.

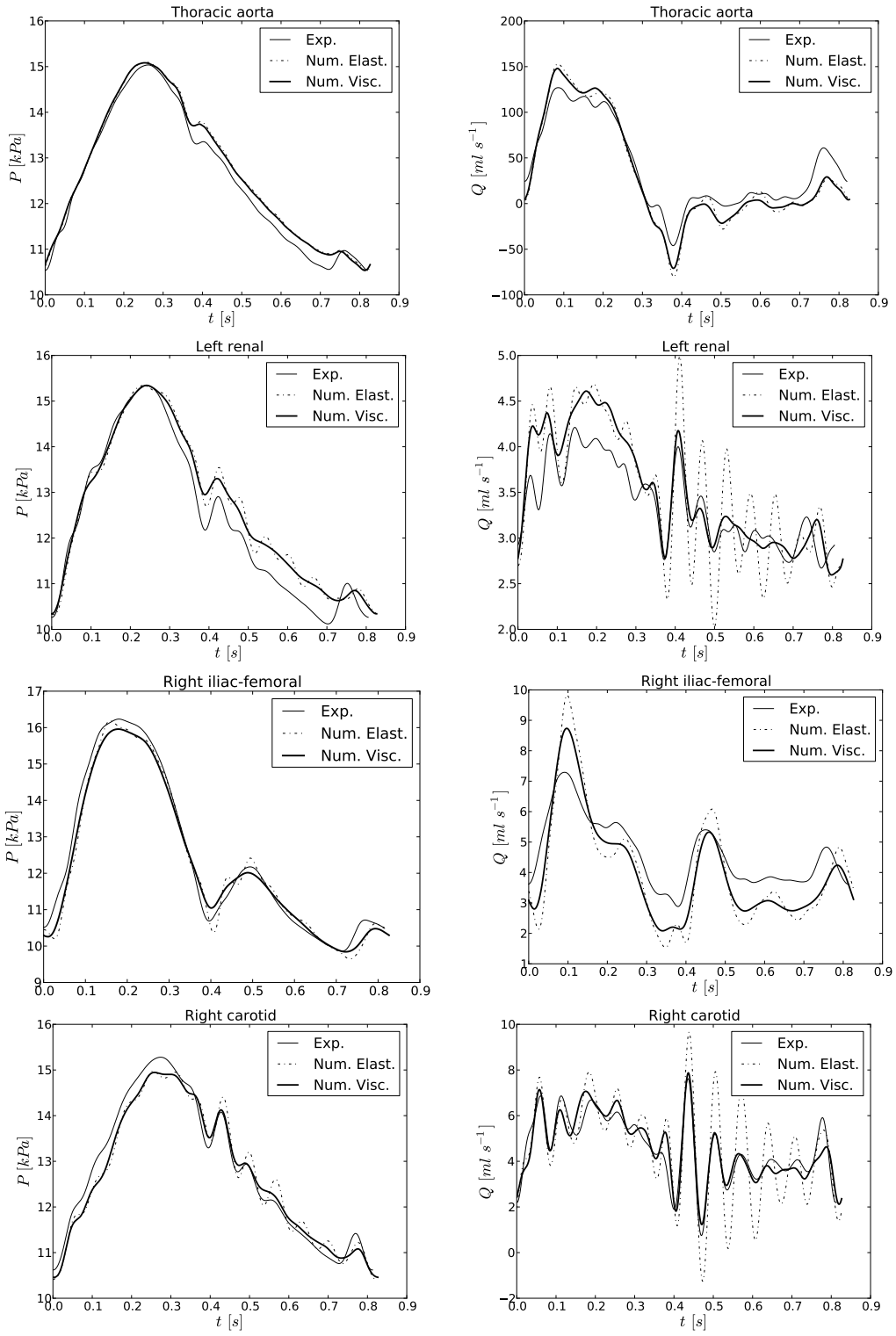

Figure 1: Comparison of numerical results obtained with a third order numerical scheme for the elastic model (dashed line) and the viscoelastic model with a relaxation time $\varepsilon = 10^{-3}\,s$ (thick continuous line) and experimental measurements (thin continuous line) reported in [2].

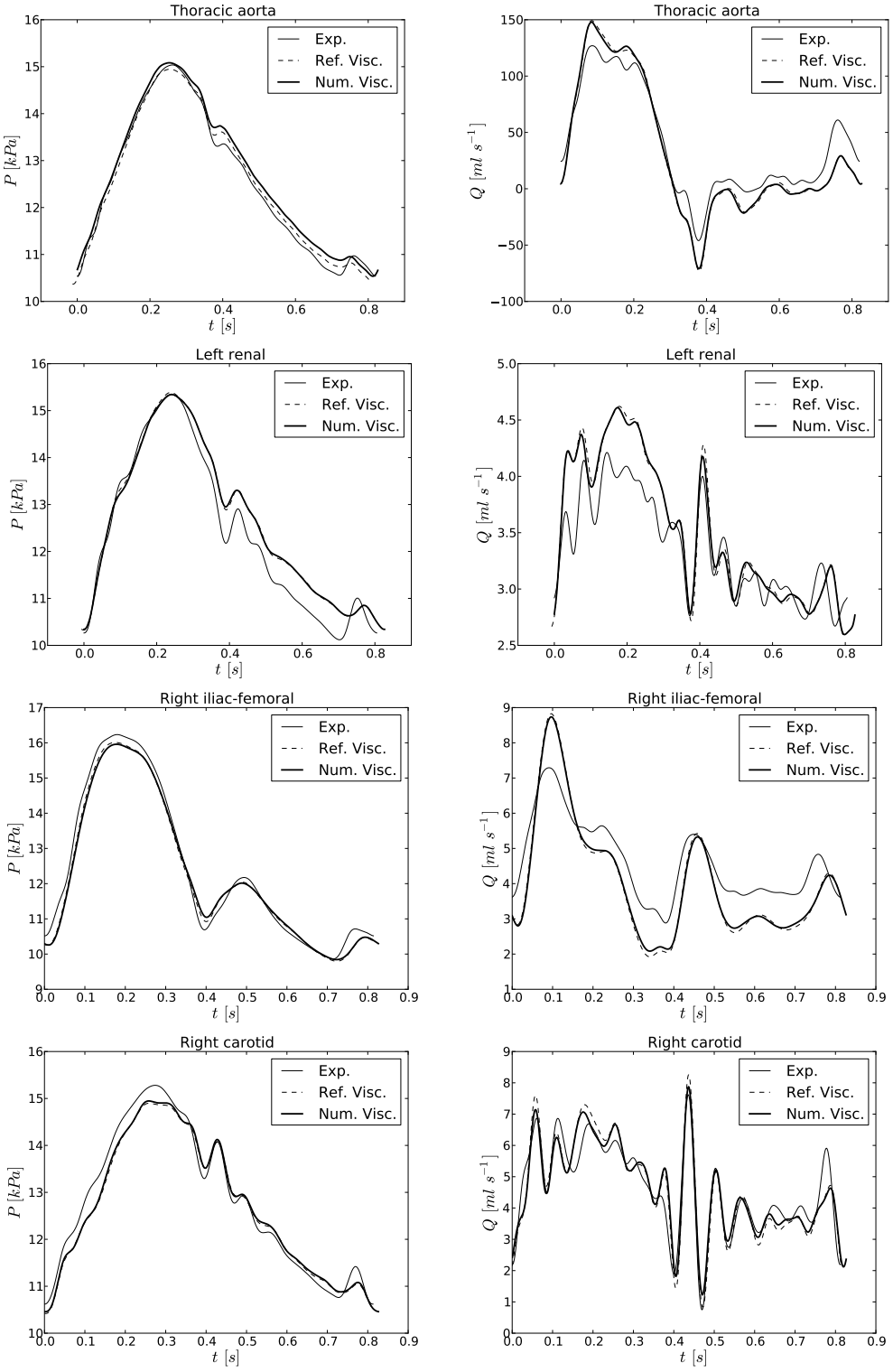

Figure 2: Comparison of numerical results obtained with our third order numerical scheme for the viscoelastic model with a relaxation time $\varepsilon = 10^{-3}\,s$ (thick continuous line), reference numerical results (dashed line) and experimental measurements (thin continuous line), both reported in [2].

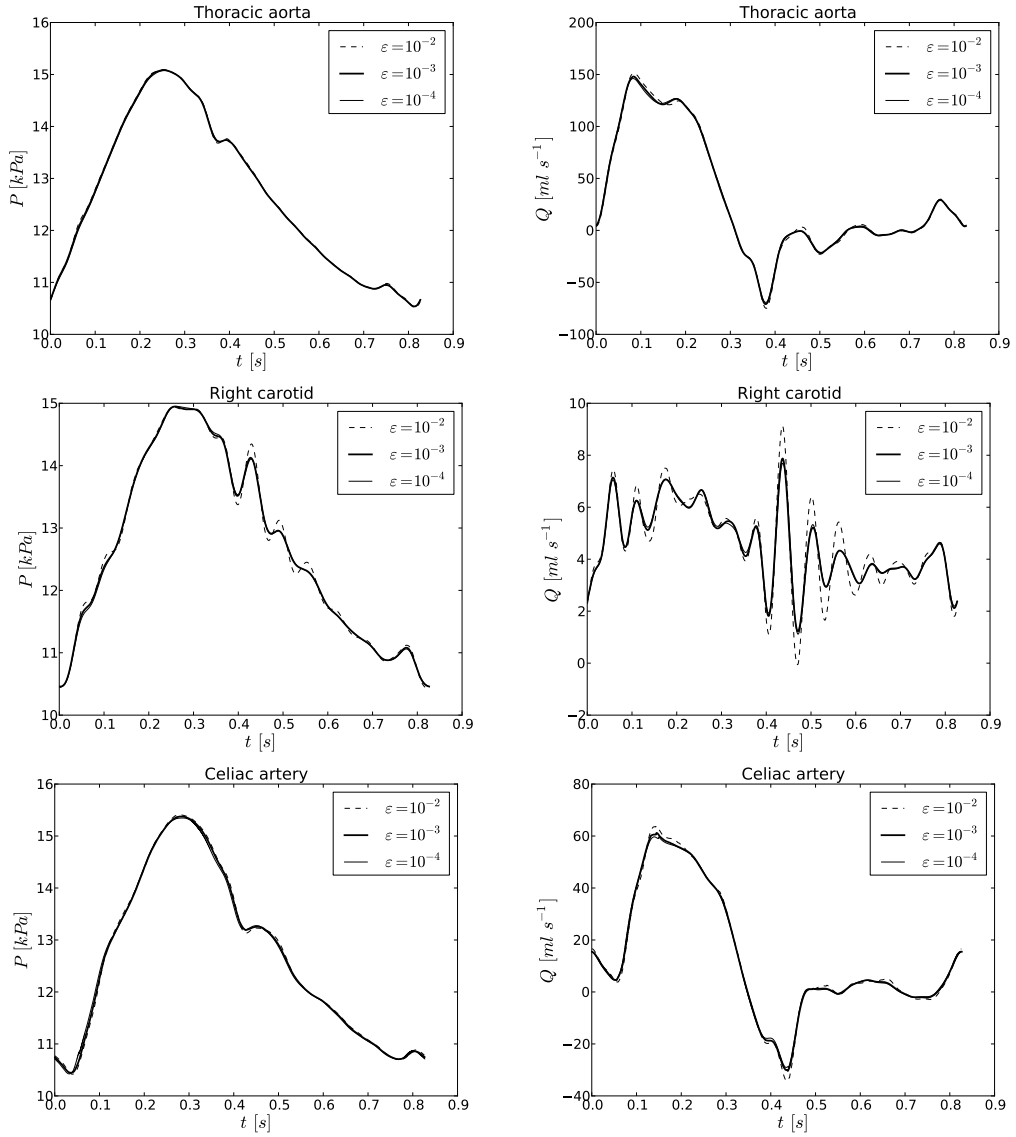

Figure 3: Comparison of numerical results obtained with our third order numerical scheme for the viscoelastic model with relaxation times $\varepsilon = 10^{-2}\,s$ (dashed line), $\varepsilon = 10^{-3}\,s$ (thick continuous line) and $\varepsilon = 10^{-4}\,s$ (thin continuous line).

A Junctions and boundary conditions

While blood flow within each vessel is modelled using equations (20), we still need to treat boundary conditions arising from measurements to be prescribed or from the interaction of one-dimensional vessels with lumped parameter models [4]. Here we briefly explain how to treat junction and to assign boundary conditions for the one-dimensional model. Details on the numerical treatment of lumped parameter models can be found in [4, 39].

A.1 Junction treatments

Let us consider a junction to be the point where J+1 vessels are confluent, where $\mathbf{Q}_j$ is the state vector associated to vessel j-th, with $j = 0,\dots,J$, see Figure 4.We assume that at the junction

$$dA_0 = dK = dp_e = 0 \tag{96}$$

and that the vessel wall has elastic properties, as proposed in [39]. We want to find state vectors $\mathbf{Q}_j^* = [A_j^*, q_j^*]$ to be used as boundary conditions for each vessel. Therefore, for $J+1$ vessels we need to compute $2(J+1)$ unknowns. $J+1$ equations are provided by requiring mass conservation

$$\sum_{j=0}^{J} g_j\, q_j^* = 0 \tag{97}$$

and continuity of total pressure

$$\tilde{p}_0^* + \frac{1}{2}\rho\left(\frac{q_0^*}{A_0^*}\right)^2 - \tilde{p}_j - \frac{1}{2}\rho\left(\frac{q_j}{A_j}\right)^2 = 0, \quad j = 1,\dots,J\,. \tag{98}$$

In (97) g_j is given as

$$g_j(I_j) = \begin{cases} 1, & \text{if } I_j = N_j\,, \\ -1, & \text{if } I_j = 1\,, \end{cases} \tag{99}$$

where I_j is the index of the computational cell of the j-th vessel that shares an interface with the junction and N_j is the number of computational cells of vessel j. Finally, the missing $J+1$ equations are provided by Riemann invariants for waves leaving the one-dimensional domain

$$\frac{q_j^*}{A_j^*} + g_j \int_{A_0}^{A_j^*} \frac{c(A)}{A} dA - \frac{q_j}{A_j} - g_j \int_{A_0}^{A_j} \frac{c(A)}{A} dA = 0 \quad j = 0,\dots,J\,. \tag{100}$$

Equations (97), (98) and (100) constitute a non-linear system with $2(J+1)$ equations and $2(J+1)$ unknowns and is solved using a Newton method. For further details on this methodology see [53].

A.2 Assigning boundary conditions for the one-dimensional model

Let $\mathbf{Q} = [A_{1D}, q_{1D}]^T$ be the state of a computational cell at the extremity of a one-dimensional vessel sharing a boundary, where we want to prescribe the cross-sectional area A_{bc}, the flow rate q_{bc}, or both of them. These quantities might arise from lumped parameter models, from measurements or from coupling conditions at junctions. If only one component of $\mathbf{Q}$ is known we compute the value of the remaining component by solving the following equation

$$\frac{q_{1D}}{A_{1D}} + g_{1D} \int_{A_0}^{A_{1D}} \frac{c(A)}{A} dA - \frac{q_{bc}}{A_{bc}} - g_{1D} \int_{A_0}^{A_{bc}} \frac{c(A)}{A} dA = 0\,, \tag{101}$$

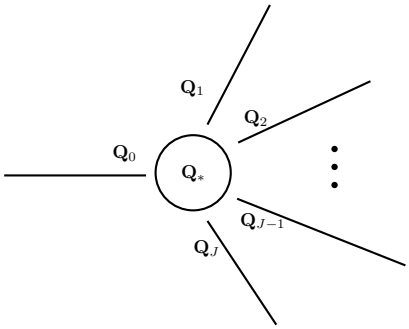

Figure 4: Schematic representation of a junction.

for the unknown quantity. Here, g_{1D} plays the role of g_j in (99), i.e. it identifies if computational cell at the extremity corresponds to the beginning or to the end of the vessel.

We denote by $\mathbf{Q}^L_{bc} = [A^L_{bc}, q^L_{bc}]^T$ and $\mathbf{Q}^R_{bc} = [A^R_{bc}, q^R_{bc}]^T$ the state vectors for boundary conditions on the left and right boundaries of the vessel, obtained from (101). To prescribe these values at the vessel extremities, we use the fluctuations

$$\mathcal{D}^+_{1-\frac{1}{2}} = f(\mathbf{Q}^L_{1D}) - f(\mathbf{Q}^L_{bc}), \qquad \mathcal{D}^-_{N+\frac{1}{2}} = f(\mathbf{Q}^R_{bc}) - f(\mathbf{Q}^R_{1D}), \tag{102}$$

where f is a flux to be determined, N is the total number of cells of the vessel and $\mathbf{Q}^{L,R}_{1D}$ are the state vectors inside the computational domain for the left and right boundaries, respectively. Moreover, assuming

$$dA_0 = dK = dp_e = d\Psi = 0\,, \tag{103}$$

from the momentum equation in (20) f must satisfy

$$f_A \partial_x A + f_q \partial_x q = \Big(c^2 - u^2 + \frac{a_\Gamma}{2}\Big)\partial_x A + \Big(2u\Big)\partial_x q = 0\,. \tag{104}$$

The reader can check that this is an exact differential equation. Therefore, flux f is found simply from integration of (104), yielding

$$f(A,q) = A\left[\frac{K}{\rho}\left(\frac{m}{m+1}\left(\frac{A}{A_0}\right)^m - \frac{n}{n+1}\left(\frac{A}{A_0}\right)^n\right) + u^2 + a_\Gamma\right]. \tag{105}$$

This procedure ensures exact mass conservation over the network at a discrete level.

References

[1] R. Abgrall and S. Karni. Two-layer shallow water system: A relaxation approach. *SIAM Journal on Scientific Computing*, 31(3):1603–1627, 2009.

[2] J. Alastruey, A. W. Khir, K. S. Matthys, P. Segers, S. J. Sherwin, P. R. Verdonck, K. H. Parker, and J. Peiró. Pulse wave propagation in a model human arterial network: Assessment of 1-d visco-elastic simulations against in vitro measurements. *Journal of Biomechanics*, 44:2250–2258, 2011.

[3] J. Alastruey, K. H. Parker, J. Peiró, S. M. Byrd, and S. J. Sherwin. Modelling the circle of Willis to assess the effects of anatomical variations and occlusions on cerebral flows. *Journal of Biomechanics*, 40:1794–1805, 2007.

[4] J. Alastruey, K. H. Parker, J. Peiró, and S. J. Sherwin. Lumped parameter outflow models for 1-d blood flow simulations: Effect on pulse waves and parameter estimation. *Communications in Computational Physics*, 4:317–336, 2008.

[5] M. Ben-Artzi and J. Falcovitz. A second order godunov–type scheme for compressible fluid dynamics. *Journal of Computational Physics*, 55:1–32, 1984.

[6] P. J. Blanco, M. R. Pivello, S. A. Urquiza, and R. A. Feijóo. On the potentialities of 3D-1D coupled models in hemodynamics simulations. *Journal of Biomechanics*, 42:919–930, 2009.

[7] S. Boscarino, L. Pareschi, and G. Russo. Implicit–explicit Runge-Kutta schemes for hyperbolic systems and kinetic equations in the diffusion limit. *SIAM Journal on Scientific Computing*, 35:22–51, 2013.

[8] S. Boscarino and G. Russo. Flux–explicit IMEX Runge-Kutta schemes for hyperbolic to parabolic relaxation problems. *SIAM Journal on Numerical Analysis*, 51(1):163–190, 2013.

[9] B. S. Brook, S. A. E. G. Fallen, and T. J. Pedley. Numerical solutions for unsteady gravity-driven flows in collapsible tubes: evolution and roll-wave instability of a steady state. *Journal of Fluid Mechanics*, 396:223–256, 1999.

[10] A. Canestrelli, A. Siviglia, M. Dumbser, and E. F. Toro. Well-balanced high-order centred schemes for non-conservative hyperbolic systems. Applications to shallow water equations with fixed and mobile bed. *Advances in Water Resources*, 32(6):834 – 844, 2009.

[11] C. E. Castro. *High–order ADER FV/DG numerical methods for hyperbolic equations*. PhD thesis, Department of Civil and Environmental Engineering, University of Trento, Italy, 2007.

[12] C. E. Castro and E. F. Toro. Solvers for the high–order Riemann problem for hyperbolic balance laws. *Journal of Computational Physics*, 227:2481–2513, 2008.

[13] C. Cattaneo. Sulla conduzione del calore. *Atti del Seminario Matematico e Fisico dell'Universita di Modena*, 3:83–101, 1948.

[14] C. Cattaneo. A form of heat-conduction equations which eliminates the paradox of instantaneous propagation. *Comptes Rendus de l'Académie des Sciences, Paris*, 247:431–433, 1958.

[15] G. Dal Maso, P. G. LeFloch, and F. Murat. Definition and weak stability of nonconservative products. *Journal de Mathématiques Pures et Appliquées*, 74:483–548, 1995.

[16] M. Dumbser. *Arbitrary high order schemes for the solution of hyperbolic conservation laws in complex domains*. PhD thesis, Institut für Aero- und Gasdynamik, Universität Stuttgart, Germany, 2005.

[17] M. Dumbser. Building blocks for arbitrary high order discontinuous Galerkin schemes. *Journal of Scientific Computing*, 27:215–230, 2006.

[18] M. Dumbser. Arbitrary high order PNPM schemes on unstructured meshes for the compressible Navier-Stokes equations. *Computers & Fluids*, 39:60 –76, 2010.

[19] M. Dumbser, D. Balsara, E. F. Toro, and C. D. Munz. A Unified Framework for the construction of one–step finite–volume and discontinuous Galerkin schemes. *Journal of Computational Physics*, 227:8209–8253, 2008.

[20] M. Dumbser, M. Castro, C. Parés, and E. F. Toro. ADER schemes on unstructured meshes for nonconservative hyperbolic systems: Applications to geophysical flows. *Computers & Fluids*, 38(9):1731 – 1748, 2009.

[21] M. Dumbser, C. Enaux, and E. F. Toro. Finite volume schemes of very high order of accuracy for stiff hyperbolic balance laws. *Journal of Computational Physics*, 227(8):3971–4001, 2008.

[22] M. Dumbser, A. Hidalgo, M. Castro, C. Parés, and E. F. Toro. FORCE schemes on unstructured meshes II: Non-conservative hyperbolic systems. *Computer Methods in Applied Mechanics and Engineering*, 199(9–12):625 – 647, 2010.

[23] M. Dumbser and C. D. Munz. ADER discontinuous Galerkin schemes for aeroacoustics. *Comptes Rendus Mécanique*, 333:683–687, 2005.

[24] M. Dumbser and E. F. Toro. A simple extension of the Osher Riemann solver to non-conservative hyperbolic systems. *Journal of Scientific Computing*, 48:70–88, 2010.

[25] M. Dumbser and E. F. Toro. On universal Osher-type schemes for general nonLinear hyperbolic conservation laws. *Communications in Computational Physics*, 10(3):635–671, 2011.

[26] S. K. Godunov. A Finite Difference Method for the Computation of Discontinuous Solutions of the Equations of Fluid Dynamics. *Matematicheskii Sbornik*, 47:357–393, 1959.

[27] H. Gómez, I. Colominas, F. Navarrina, and M. Casteleiro. A generalized method for advective-diffusive computations in engineering. In required, editor, *Fluid Structure Interaction and Moving Boundary Problems*, pages 563–572. Chakrabarti S. K., Hernandez S., Brebbia C. A., Southampton, UK., 2005.

[28] H. Gómez, I. Colominas, F. Navarrina, and M. Casteleiro. A finite element formulation for a convection-diffusion equation based on cattaneo's law. *Computer Methods in Applied Mechanics and Engineering*, 196:1757–1766, 2007.

[29] L. Grinberg, E. Cheever, T. Anor, J. R. Madsen, and G. E. Karniadakis. Modeling Blood Flow Circulation in Intracranial Arterial Networks: A Comparative 3D/1D Simulation Study. *Annals of Biomedical Engineering*, 2010.

[30] A. Harten, B. Engquist, S. Osher, and S. R. Chakravarthy. Uniformly high order accuracy essentially non–oscillatory schemes III. *Journal of Computational Physics*, 71:231–303, 1987.

[31] A. Hidalgo and M. Dumbser. ADER schemes for nonlinear systems of stiff advection-diffusion-reaction equations. *Journal of Scientific Computing*, 48:173–189, 2011.

[32] A. Hidalgo, L. Tello, and E. F. Toro. Numerical and analytical study of an atherosclerosis inflammatory disease model. *Journal of Mathematical Biology*, 2013. In Press.

[33] G. S. Jiang and C. W. Shu. Efficient implementation of weighted ENO schemes. *Journal of Computational Physics*, 126:202–228, 1996.

[34] S. Jin, L. Pareschi, and G. Toscani. Diffusive relaxation schemes for multiscale discrete-velocity kinetic equations. *SIAM Journal on Numerical Analysis*, 35(6):2405–2439, 1998.

[35] S. Jin and Z. Xin. The relaxation schemes for systems of conservation laws in arbitrary space dimensions. *Communications on Pure and Applied Mathematics*, 48:235–277, 1995.

[36] M. Käser. *Adaptive methods for the numerical simulation of transport processes*. PhD thesis, Institute of Numerical Mathematics and Scientific Computing, University of Munich, Germany, 2003.

[37] M. Käser. ADER schemes for the solution of conservation laws on adaptive triangulations. Mathematical Methods and Modelling in Hydrocarbon Exploration and Production. Springer–Verlag, Vol. 7, 2004.

[38] F. Y. Liang, S. Takagi, R. Himeno, and H. Liu. Multi-scale modeling of the human cardiovascular system with applications to aortic valvular and arterial stenoses. *Medical and Biological Engineering and Computing*, 47:743–755, 2009.

[39] K. S. Matthys, J. Alastruey, J. Peiró, A. W. Khir, P. Segers, P. R. Verdonck, K. H. Parker, and S. J. Sherwin. Pulse wave propagation in a model human arterial network: Assessment of 1-D numerical simulations against *in vitro* measurements. *Journal of Biomechanics*, 40:3476–3486, 2007.

[40] G. Montecinos, C. E. Castro, M. Dumbser, and E. F. Toro. Finite volume schemes for very high order of accuracy for stiff hyperbolic balance laws. *Journal of Computational Physics*, 231:6472–6494, 2012.

[41] L. O. Müller, C. Parés, and E. F. Toro. Well-balanced high-order numerical schemes for one-dimensional blood flow in vessels with varying mechanical properties. *Journal of Computational Physics*, 242:53 – 85, 2013.

[42] L. O. Müller and E. F. Toro. Well-balanced high-order solver for blood flow in networks of vessels with variable properties. *International Journal for Numerical Methods in Biomedical Engineering*, 2013. In Press.

[43] L. O. Müller and E. F. Toro. A global multiscale mathematical model for the human circulation with emphasis on the venous system. *International Journal for Numerical Methods in Biomedical Engineering*, pages n/a–n/a, 2014.

[44] G. B. Nagy, O. E. Ortiz, and O. A. Reula. The behaviour of hyperbolic heat equations solutions near their parabolic limit. *Journal of Mathematical Physics*, 8:4334–4356, 1994.

[45] H. Nishikawa. A first-order system approach for diffusion equation. II: Unification of advection and diffusion. *Journal of Computational Physics*, 229:3989–4016, 2010.

[46] H. Nishikawa. New-generation hyperbolic Navier-Stokes schemes: O(1/h) Speed-up and accurate viscous/heat fluxes. In *20th AIAA Computational Fluid Dynamics Conference, 27 - 30 June, Honolulu, Hawaii, 2011*, 2011.

[47] H. Nishikawa and P. L. Roe. Towards High-Order Fluctuation-Splitting Schemes for Navier-Stokes Equations. In *17th AIAA Computational Fluid Dynamics Conference. 6 - 9 June 2005, Toronto, Ontario Canada*, 2005.

[48] H. Nishikawa and P. L. Roe. On high-order fluctuation-splitting schemes for navier-stokes equations. In Clinton Groth and DavidW. Zingg, editors, *Computational Fluid Dynamics 2004*, pages 799–804. Springer Berlin Heidelberg, 2006.

[49] C. Parés. Numerical methods for nonconservative hyperbolic systems: a theoretical framework. *SIAM Journal on Numerical Analysis*, 44:300–321, 2006.

[50] L. Pareschi and G. Russo. Implicit–explicit runge–kutta schemes and applications to hyperbolic systems with relaxation. *Journal of Scientific Computing*, 25:129–155, 2005.

[51] P. Reymond, F. Merenda, F. Perren, D. Rüfenacht, and N. Stergiopulos. Validation of a one-dimensional model of the systemic arterial tree. *American Journal of Physiology - Heart and Circulatory Physiology*, 297:H208–H222, 2009.

[52] T. Schwartzkopff, C. D. Munz, and E. F. Toro. ADER: High–order approach for linear hyperbolic systems in 2D. *Journal of Scientific Computing*, 17:231–240, 2002.

[53] S. J. Sherwin, V. Franke, J. Peiró, and K. H. Parker. One-dimensional modelling of a vascular network in space-time variables. *Journal of Engineering Mathematics*, 47:217–250, 2003.

[54] B. N. Steele, J. Wan, P. Ku, J, T. J. Hughes, and C. A. taylor. In vivo validation of a one-dimensional finite-element method for predicting blood flow in cardiovascular bypass grafts. *IEEE Transactions on Biomedical Engineering*, 50:649–655, 2003.

[55] V. A. Titarev and E. F. Toro. ADER: Arbitrary high order Godunov approach. *Journal of Scientific Computing*, 17:609–618, 2002.

[56] V. A. Titarev and E. F. Toro. High–order ADER schemes for scalar advection–reaction–diffusion equations. *CFD Journal*, 12(1):1–6, 2003.

[57] V. A. Titarev and E. F. Toro. ADER schemes for three–dimensional hyperbolic systems. *Journal of Computational Physics*, 204:715–736, 2005.

[58] E. F. Toro. *Riemann solvers and numerical methods for fluid dynamics*. Springer–Verlag, Berlin Heidelberg, Third edition, 2009.

[59] E. F. Toro and A. Hidalgo. ADER finite volume schemes for nonlinear diffusion–reaction equations. Technical Report Preprint NI07007–NPA, Newton Institute for Mathematical Sciences, University of Cambridge, UK, 2007.

[60] E. F. Toro, R. C. Millington, and L. A. M. Nejad. Towards very high–order Godunov schemes. In *Godunov Methods: Theory and Applications. Edited Review, E. F. Toro (Editor)*, pages 905–937. Kluwer Academic/Plenum Publishers, 2001.

[61] E. F. Toro and A. Siviglia. Flow in collapsible tubes with discontinuous mechanical properties: mathematical model and exact solutions. *Communications in Computational Physics*, 13(2):361–385, 2013.

[62] E. F. Toro and V. A. Titarev. Solution of the generalised Riemann problem for advection–reaction equations. *Proceedings of the Royal Society of London: A*, 458:271–281, 2002.

[63] P. Vernotte. Les paradoxes de la theorie continue de l'equation de la chaleur. *Comptes Rendus de l'Académie des Sciences, Paris*, 246:3154–3155, 1958.

[64] N. Xiao, J. Alastruey, and Alberto F. C. A systematic comparison between 1-d and 3-d hemodynamics in compliant arterial models. *International Journal for Numerical Methods in Biomedical Engineering*, pages n/a–n/a, 2013.